Final Report
NASA Cooperative·Agreement NCC2-1044

Driving Parameters for Distributed and Centralized
Air Transportation Architectures

Massachusetts Institute of Technology
International Center for Air Transportation
And
Laboratory for Information and Decision Systems

January 17, 2001

Abstract

This report considers the problem of intersecting aircraft flows under decentralized conflict avoidance rules. Using an Eulerian standpoint (aircraft flow through a fixed control volume), new air traffic control models and scenarios are defined that enable the study of long-term airspace stability problems. Considering a class of two intersecting aircraft flows, it is shown that airspace stability, defined both in terms of safety and performance, is preserved under decentralized conflict resolution algorithms. Performance bounds are derived for the aircraft flow problem under different maneuver models. Besides analytical approaches, numerical examples are presented to test the theoretical results, as well as to generate some insight about the structure of the traffic flow after resolution. Considering more than two intersecting aircraft flows, simulations indicate that flow stability may not be guaranteed under simple conflict avoidance rules. Finally, a comparison is made with centralized strategies to conflict resolution.

THIS PAGE INTENSIONALLY LEFT BLANK

Contents

Chapter 1

Introduction and Motivation

Following the sustained growth of past and forecasted air traffic, the control of air traffic is growing in importance. In the United States, the air traffic is expected to increase by 5% annually for the next 15 years [19]. Even with today's traffic, current air traffic control system has been suffering from problems like over-intensive workload of the controllers (due to the limit of the amount of information processing that a controller can afford) and common airborne delays in flights (due to congestion in the skies), *etc*. There has been a perceived need in the air traffic control for new technologies and new architectures.

1.1 Current Air Traffic System and Free Flight

Current air traffic control system of United States is organized hierarchically with a single Air Traffic Control System Command Center (ATCSCC), which supervises the overall traffic flow. The whole system consists of 22 Air Route Traffic Control Centers (ARTCCs) organized by geographical region, and each ARTCC is further divided into 20 to 50 sectors. At any time, there are about 8000 aircraft on average flying in the skies of United States (estimated from the data in [20]), and there are approximately 1500 enroute air traffic controllers, with at least one controller responsible for each sector, regulating the aircraft flow and making sure no hazardous situation develops.

The air traffic control is for the most part centralized within a given sector. The

6

centralized control directs aircraft flows along predefined air routes, and aircraft are allowed to fly only along these routes (with some exceptions). The air routes are straight line segments connecting a network of navigation beacons (VHF Omnidirectional Range (VOR) and Distance Measuring Equipment systems (DME)). These beacons are used by pilots as navigational aids to update and correct the position information. Flying on segments connecting the beacons makes the problem of aircraft navigation and automated guidance particularly easy. The network structure of the aircraft routing system allows the controllers to get *a priori* information on aircraft conflict geometries and their locations.

Many decades of working experience have demonstrated that the air traffic system with the network architecture is safe. However, the centralized control in this architecture frequently causes bottlenecks to develop. Also the air traffic system suffers from strong perceived drawbacks, such as systematic indirect routing between origin and destination, and in general a perceived lack of navigation freedom for pilots and airlines.

Recently new technologies have been proposed for application in air traffic control. For example, the new generation of Global Navigation Satellite Systems (GNSS) has in principle removed the limitation of the ground-based navigation infrastructure (one of the components of GNSS technology is the Global Positioning System (GPS)); And the improved datalink technologies have provided improved weather and traffic information to both the pilots and controllers. These technological developments have led to the possibility of developing *Free Flight* [34], a concept whereby pilots and airlines would be allowed more freedom in the decision making process.

Under Free Flight, the pilots would be able to optimize their trajectories according to several factors such as safety, weather, operating costs and coordination with other flights. Free Flight would enable greater traffic volume and complexity by distributing some of the functionality, including conflict detection and resolution, to pilots and/or airborne systems. Obviously, the operation of Free Flight greatly departs from the current, network based architecture of the aircraft traffic system. Its safety remains to be proved. For example, the lack of predictability of conflict location under Free

Flight will increase the complexity of conflict detection and resolution for human operators. In addition, the set of standards for operational concept evaluation has evolved to a more sophisticated and difficult certification process. The safety of any new air traffic system cannot rely on experience only, it should also be proved upon appropriate mathematical modeling and engineering analysis techniques. Thus, Free Flight offers a wide array of new challenges and opportunities to the research community.

1.2   Conflict Resolution

No matter in current centralized air traffic control system or in a decentralized system allowing Free Flight, the detection and resolution of conflicts is always a crucial part of the system architecture. There has been a long history of investigation on aircraft conflict detection and resolution. However, with emerging Free Flight policies, new technologies, and an increased emphasis on economic and market factors, conflict detection and resolution needs to be re-examined and updated based on new concerns and techniques.

A conflict is a loss of separation between aircraft. In an air traffic system, each aircraft is assumed to be surrounded by two virtual cylinders, the *protected zone* and *alert zone*. The radius and height of the protected zone depends on the FAA separation standards, while the shape and size of the alert zone depends on various factors, such as aircraft performance, airspeed, altitude, traffic situation, *etc.* A conflict between two aircraft is then defined as a situation in which the aircraft protected zones overlap. Correspondingly, a system of aircraft is said to be safe if the aircraft protected zones never overlap.

In recent years, a considerable body of research has been devoted to aircraft conflict prediction and resolution. Excellent overviews of the approaches for conflict prediction and resolution can be found in [24, 36].

This thesis considers the problem of air traffic "stability" under decentralized conflict detection and resolution. One of the major issues that arises is the proper

8

definition of "stability" of air traffic flows. In traditional control system terms, the notion of "stability" usually relates to the long term behavior of dynamical systems, which is expected to remain within some acceptable bounds and often to converge towards a specific desired state. For example, individual aircraft stability concepts are tied to the requirement that both aircraft attitude and position stay close enough to some reference attitude and position.

Considering problems of air traffic management, the requirement for stability becomes more complex: While aircraft are expected to follow a reference trajectory (as loosely defined as it may be), aircraft are also required to *stay away* from each other to prevent near misses or even airborne collisions. In this context it becomes quite important for the researcher to define appropriate notions of stability. This in turn entails the requirement of appropriately defining the system being worked upon. Much of the research focuses on problems involving a finite, usually small number of aircraft. Such a Lagrangian standpoint (in which few aircraft are analyzed) is useful when designing efficient conflict detection and resolution systems. However, it is not convenient to use for flow stability analyses, since interactions occurring within a finite set of aircraft can only have a finite duration.

We propose in this thesis an "Eulerian" standpoint, originally introduced in [25], whereby many aircraft flow through a well-delimited volume of airspace. The motivation behind this standpoint is that, even under Free Flight, many aircraft flow interactions are expected to occur within relatively well-defined parts of the airspace, corresponding to the intersection between one or more optimal routes linking city pairs, for example. This viewpoint is also very much compatible with an air traffic controller's current view of the air transportation system, with the volume of airspace being a sector. A recent paper adopting that standpoint is [8].

1.3   Thesis Organization

The thesis is organized as follows:

In Chapter 2, the aircraft flow models are introduced. An appropriate notion of

aircraft flow stability is defined and the decentralized strategy followed by each aircraft is introduced. In Chapter 3, a proof of aircraft flow stability is provided for the case of two intersecting aircraft flows where aircraft use a simple, decentralized control rule, and perform their conflict resolution through lateral relative position change. The results are discussed along with simulations and generalizations. Chapter 4 presents the proof of intersecting aircraft flow stability under general offset model. Simulations for both offset model and velocity change model are given in this chapter. In Chapter 5, a comparison is drawn between centralized and decentralized resolutions, where the centralized resolution strategies are realized via mixed integer linear programming. Chapter 6 is the conclusion of the thesis.

Chapter 2

Air Traffic Models and Problem Formulation

2.1 General Considerations

The definition of appropriate models is a significant challenge when considering problems in air transportation [18]. For the conflict detection and resolution problem, most researchers have traditionally concentrated on scenarios involving a *finite* number of aircraft. However, there appears to be a widespread concern about the "domino effect", whereby one conflict resolution maneuver creates new conflicts which in turn need to be solved, *etc.* In this thesis, we will concentrate on a possibly *infinite* number of aircraft flowing through a finite portion of the airspace.

The system under study consists of a given volume of airspace, and a set of aircraft flowing in and out of it, as shown in Fig. 2-1. The dynamics of the system are determined by the "boundary conditions" that indicate the location, speed and rate at which aircraft appear in the volume of airspace, and by their individual behavior while they fly within the airspace. Clearly, some boundary conditions are unacceptable, *e.g.*, the case when two aircraft appear into the control region very close to each other and on a head-on collision course. Since relatively little is known about interacting aircraft flows, we will consider aircraft flows with low complexity.

The aircraft are assumed to be *intelligent*, *i.e.*, their pilots actively attempt to
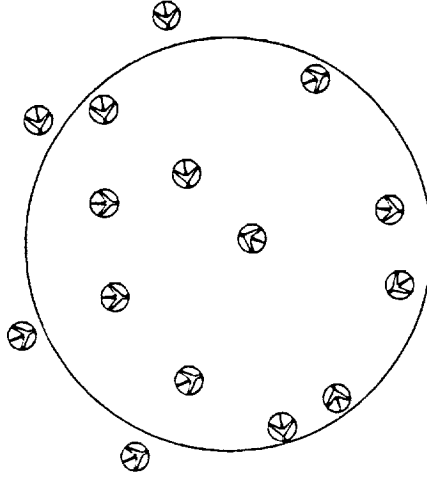
Figure 2-1: Aircraft flowing in and out of "control volume".

maneuver and avoid conflicts at the smallest possible cost.

2.2 Aircraft Maneuver Models

Although designing and analyzing systems for aircraft conflict detection and resolution needs to account for the three dimensions, this thesis only investigates air traffic evolving in two dimensions (planar conflict resolution): The trajectories of all aircraft are assumed to evolve in the horizontal plane. While vertical maneuvers appear to be most efficient for tactical conflict resolution (such as in the case of TCAS (Traffic Alert and Collision Avoidance System)), horizontal maneuvers might be more appropriate for the "strategic" conflict resolution context considered in this thesis, because they induce less passenger discomfort and they do not require flight level changes and thus may not perturb the vertically stratified traffic structure as it exists today in the enroute airspace.

This thesis will be concerned with very simple aircraft behaviors. In particular aircraft fly only along straight and level trajectories. Moreover, we will assume that only one conflict area exists, and that aircraft may perform only one conflict avoidance maneuver [2].

Two models for conflict avoidance will be considered in this thesis; Fig. 2-2 illustrates these conflict resolution models.

12
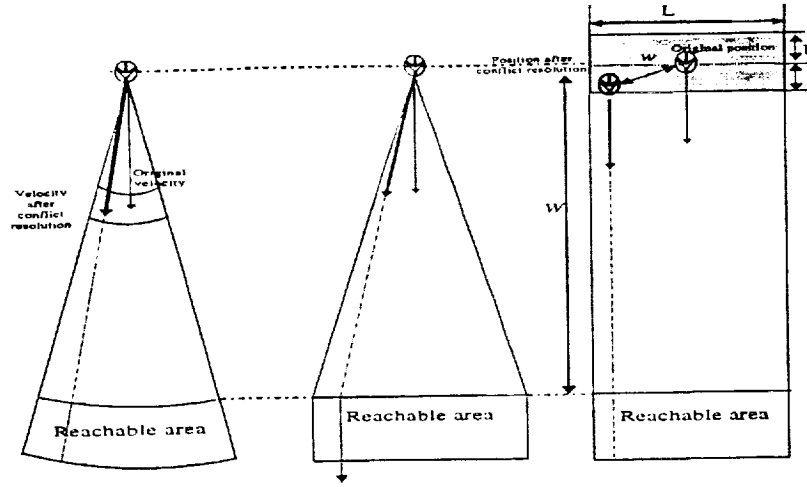
Figure 2-2: Velocity change model v.s. offset model. Left: The aircraft maneuver is an immediate horizontal velocity change. Middle: The aircraft maneuver is a velocity change followed by a second velocity change. Right: The aircraft maneuver is a relative position change.

- Velocity change model: In this model (left picture in Fig. 2-2), both heading changes and speed changes are used to modify aircraft trajectories. Following the approach of Andrews [2], the velocity changes are assumed to occur instantaneously when the aircraft makes a decision. This model will be used for simulation purposes.

- Offset model: This model (right picture in Fig. 2-2), used for analysis and simulation, consists of modeling aircraft trajectory changes via both lateral and longitudinal relative position changes, the speed vector remaining the same before and after the position changes. This model appears to be less realistic than the previous model; however, it generates a far simpler analytic framework. In addition, the offset model can be seen as a good approximate model for the velocity change model: If we allow the speed and heading (in the velocity change model) to change independently within specified bounds, and at the same time we allow the lateral and longitudinal displacement (in the offset model) to vary independently within given bounds, then for a given time horizon T, the areas reached after both velocity change and relative position change are similar in shape, especially for small deviations. As shown in Fig. 2-2, we denote b and f as the allowed largest backward and forward displacements of the aircraft. In

13

practice, T would be chosen to be the mean time to conflict. Alternatively, the offset model can also be considered to be a close approximation of the "offset maneuver model" shown in the middle of Fig. 2-2 and used in [11]. In this model, the aircraft initially changes speed and heading as in the velocity change model and then resumes original speed and heading after traveling the distance W, shown in Fig. 2-2. Considering enroute aircraft with an approximate velocity of 450 knots and an approximate time to conflict $T = 10$ minutes, the distance to conflict W is approximately 75 nautical miles (nm). Considering a velocity change model allowing for ± 10 degrees heading change and a $\pm 7\%$ velocity change, the corresponding offset model would allow for a lateral displacement bound of ± 13 nm and longitudinal displacement bound of approximately ± 5 nm.

2.3   Aircraft Flow Arrival Geometry

The basic aircraft flow model chosen in this thesis is that shown in Fig. 2-3, originally introduced by Niedringhaus in [29]. Two aircraft streams, oriented at a given angle θ ($\theta = 90$ degrees in Fig. 2-3) relative to each other, feed aircraft into a circular conflict area. The streams are organized in such a way that all aircraft within each stream are originally headed in the same direction. For simplicity of exposition only, it will also be assumed all aircraft fly at the same speed, and originally all aircraft in each stream fly along the same track prior to entering the control volume. The spacing between each aircraft in each flow is arbitrary but no less than a given minimum safe distance d (in practice $d = 5$ nm). Let $E_1, E_2, \ldots, E_i, \ldots$ be the eastbound aircraft entering the control volume, and $S_1, S_2, \ldots, S_j, \ldots$ the southbound aircraft, where aircraft are indexed according to the order they entered the control volume.

Generalizations will also be made to the above aircraft flow model in this thesis: We will consider conflict scenarios involving arbitrary encounter angles, different times to conflict, different aircraft speeds and multiple aircraft flows.

14
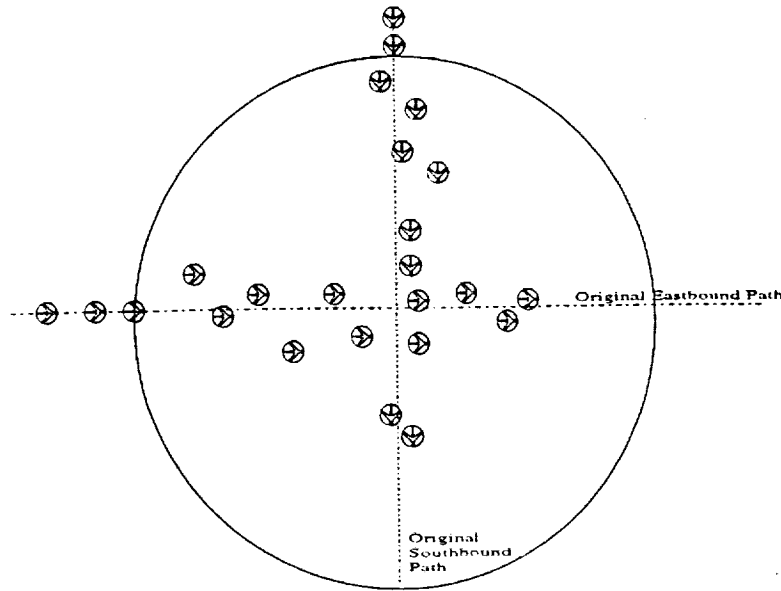
Figure 2-3: Two crossing aircraft flows.

2.4 Conflict Resolution Rules and Maneuver

A conflict is declared whenever the projected straight path of any aircraft pair leads them to a miss distance that is less than *d*. The decentralized conflict resolution scheme chosen in this thesis follows a sequential approach, whereby aircraft solve potential conflicts one at a time. To simplify matters, it is assumed that the order in which aircraft perform their resolution maneuver is the same as the order they enter the circular conflict area, although this assumption could be relaxed. An aircraft solving a conflict considers all other aircraft that maneuvered before it as moving obstacles, but does not account for the aircraft which have not maneuvered yet. Thus each aircraft has knowledge of all aircraft that have already performed a maneuver (or decided that no maneuver was necessary). A reliable implementation of such sequential approaches is described in [1].

Given those aircraft which have already performed a resolution maneuver (and must therefore be considered as obstacles), the resolution maneuver for the next aircraft scheduled for conflict resolution will be such that (i) after the resolution no conflict exists between this scheduled aircraft and any of the aircraft which have already performed resolution maneuvers, and (ii) the amplitude of the conflict avoidance maneuver is as small as possible.

15

2.5 Notions of Stability

In this thesis, the system will be stable if:

1. No conflict occurs among aircraft at any time, that is, all conflicts are resolved and do not create any new, unsolvable conflicts.

2. The deviation of the aircraft trajectory from nominal, due to the requirement for conflict resolution, remains bounded.

This definition summarizes the two most important requirements in air traffic control: Guaranteed safety and efficiency of traffic handling.

Chapter 3

Aircraft Flow Stability under Lateral Offset Model and Heading Control Model

This chapter analyzes the aircraft flow stability for the lateral offset model and heading control (or heading change) model. These two models are special cases of the offset model and velocity change model: In the heading control model, the velocity change of an aircraft is restricted to heading changes only, with no speed change, while in the lateral offset model, aircraft trajectory changes via a single lateral position change. General discussions on the offset model and velocity change model will be given in the next chapter.

As we have mentioned in the previous chapter, the resolution maneuver for the aircraft scheduled for conflict resolution will be such that the amplitude of the conflict avoidance maneuver is as small as possible. For the heading control model, the resolution maneuver will be to minimize the deviation from the nominal heading. Similarly, for the lateral offset model, the resolution maneuver will attempt to minimize the lateral position change necessary for conflict resolution. In the computer simulations presented thereafter, both conflict resolution maneuvers (heading change and lateral position change) are generated by a simple line search away from the nominal heading and position, using a predefined step size.

17

3.1 Closed-loop System Stability for Lateral Offset Model

This section presents one of the main results of this chapter: The system shown in Fig. 2-3, under the conflict resolution rule described above, is stable. More precisely, we ask the following question: Assuming the system has been running correctly in the past, will it keep running correctly in the future? Indeed, it is possible to construct "initial conditions" for the system such that conflicts are unavoidable. We now show that an incoming aircraft (bold in Fig. 3-1) can always find a conflict resolution maneuver and proceed with a conflict-free trajectory.

In this section, we will assume that aircraft resolve conflicts via lateral position changes. The lateral offset model can be treated as a close approximation of the heading control model. The advantage of the offset model is its simplicity of use for analysis purposes.

3.1.1 Conflict Geometry

For simplicity, we assume that the two crossing aircraft flows are oriented 90 degrees with respect to each other, with one southbound and one eastbound aircraft flow, as shown in Fig. 3-1. Also, we will assume that all aircraft initially follow each other along two intersecting lines, and that after maneuvering, all aircraft remain within a "maneuver corridor" of total width L centered along the nominal paths. These assumptions may be relaxed, and some generalizations could be found in Section 3.3.

Without loss of generality, one may assume that the next aircraft to perform a resolution maneuver is eastbound, as represented in bold in Fig. 3-1. By definition of the aircraft flow and allowable maneuvers, this aircraft never conflicts with neighboring eastbound aircraft. In addition, each southbound aircraft within the control volume has already performed a resolution maneuver and must be considered as a moving obstacle.

To obtain a clear understanding of the conflict geometry, we introduce the follow-
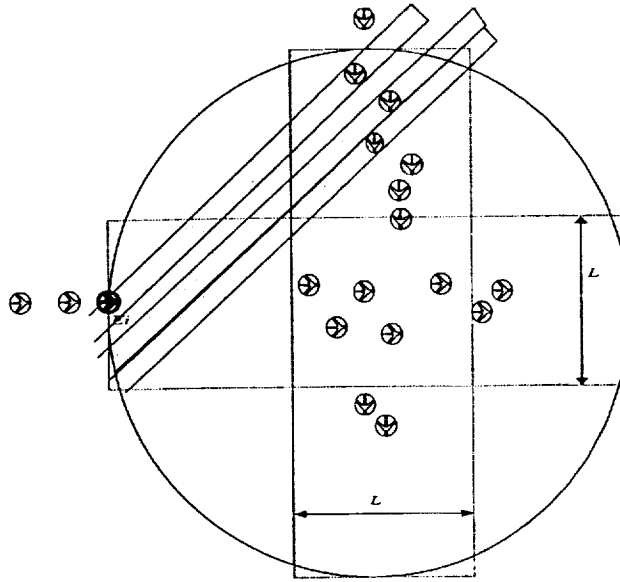
Figure 3-1: Aircraft flow configuration for stability analysis. The shaded areas are locations where a conflict will occur.

ing two concepts: *aisle* and *protected circle*.

Each aircraft projects a linear, slab-shaped virtual *"aisle"* of width d, centered around the aircraft and inclined 45 degrees (denoted in light grey in Fig. 3-1). For general encounter angles and aircraft speeds, this aisle is oriented along the relative velocity vectors. For the aircraft in the two streams to avoid any conflict, they must maneuver so that the aisles defined by the eastbound aircraft do not overlap any of the aisles of the southbound aircraft. Failure to do so means that a conflict will occur. At the same time, the aisles of the aircraft in the same stream may overlap, and therefore they may form a joint aisle. For example, the aisles of two aircraft that are in contact with each other form a joint aisle, the width of which ranges from d to $2d$.

A *protected circle* is an imaginary circle of radius $d/2$ centered around an aircraft (note that the size of the aircraft drawn in all figures is considerably exaggerated). Obviously, the protect circles of any pair of aircraft should not overlap, currently or in the future. Otherwise, a conflict will occur. Also for an aircraft in one stream to to avoid conflict with the aircraft in the other stream, it must maneuver so that its protected circle does not intersect the aisles of any aircraft in the other stream. Without causing confusion, we use the same notation (*e.g.* E_i) to represent an aircraft
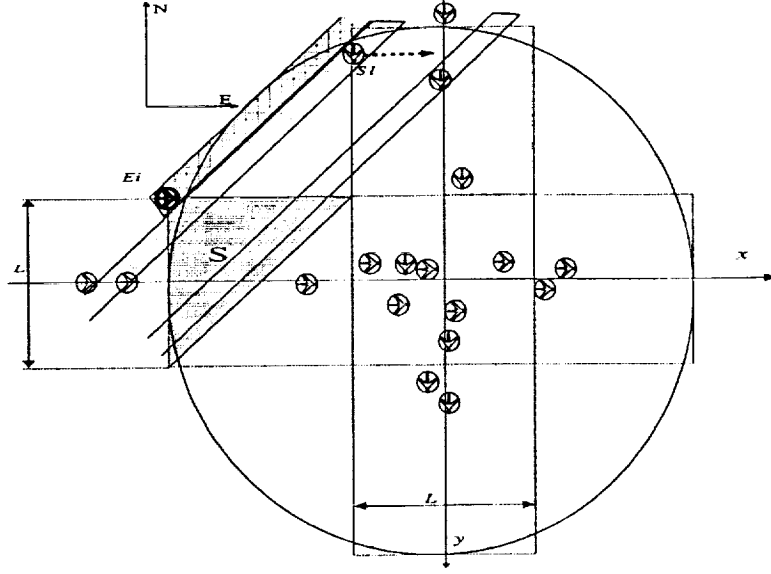
Figure 3-2: Existence of conflict resolution maneuver is enabled by intelligent behavior.

and its corresponding protected circle. And we do not distinguish the following two expressions: "the protected circle of aircraft A is in contact with the protected circle of aircraft B" and "aircraft A is in contact with aircraft B".

3.1.2 Existence of Conflict Resolution Maneuver

It is now shown that an aircraft entering the control volume (e.g., the eastbound aircraft E_i indicated in bold in Fig. 3-2) can always execute a lateral displacement maneuver that results in a conflict-free trajectory, if the width of the maneuver corridor, L, is sufficiently large. We begin with the hypothesis that such a maneuver does *not* exist, and then make the following argument:

The aisles of the eastbound aircraft which are ahead of E_i should not cover the protected circle of E_i, wherever E_i is located within the maneuver corridor. Otherwise, aircraft E_i could hide inside one of such aisles, and therefore, succeed in finding a lateral displacement (less than $L/2$) that results in a conflict-free trajectory. In other words, there should not exist any aircraft other than E_i in the area of the shaded right triangle S as seen in Fig. 3-2.

At the same time, all southbound aircraft currently inside the control volume have already performed minimum lateral displacement conflict resolution maneuvers, and

are flying along straight, conflict-free southbound paths. By hypothesis, their aisles intersect the protected circle E_i, wherever its location is, since no conflict resolution is possible. In particular, at least one aisle intersects the protected circle E_i when E_i deviates fully to the left, as shown in Fig. 3-2. For this to happen, the corresponding southbound aircraft (denoted by S_l) must have deviated to the right (from its nominal path) by a distance larger than $L/2 - \sqrt{2}d$.

Assume

$$L > 2\sqrt{2}d. \tag{3.1}$$

From the above argument about the eastbound aircraft, we see that the aisles of the eastbound aircraft should not intersect the protected circle of S_l if S_l were shifted a lateral displacement of $L/2 - \sqrt{2}d$ closer to the central axis of the maneuver corridor. Thus, we get a conflict-free resolution maneuver for S_l with smaller amplitude. This causes contradiction with the statement that the southbound aircraft have already performed minimum lateral displacement maneuvers.

Therefore, there must exist a conflict avoidance maneuver for E_i, and the closed-loop system is therefore stable.

The above argument has also provided an upper bound on the maximum conflict avoidance maneuver amplitude for both southbound and eastbound aircraft: The maximum lateral deviation experienced by the aircraft is bounded above by $\sqrt{2}d$. If $d = 5$ nm (nautical miles), the lateral deviations will not be larger than 7.1 nm. Considering a scenario where conflicts are predicted and solved 20 minutes ahead of time, and aircraft flying at 500 knots, the corresponding distance to conflict R is approximately 160 nm. Thus an equivalent maximum heading change amplitude would be approximately 2.5 degrees.

Now let us look at a very simple situation involving only two aircraft: An eastbound aircraft and a southbound aircraft arrive in the conflict area at the same time. Without loss of generality, we assume that the southbound aircraft makes decision and maneuver first. Since in our conflict resolution rules an aircraft does not account for the aircraft which have not maneuvered yet, the southbound aircraft need not
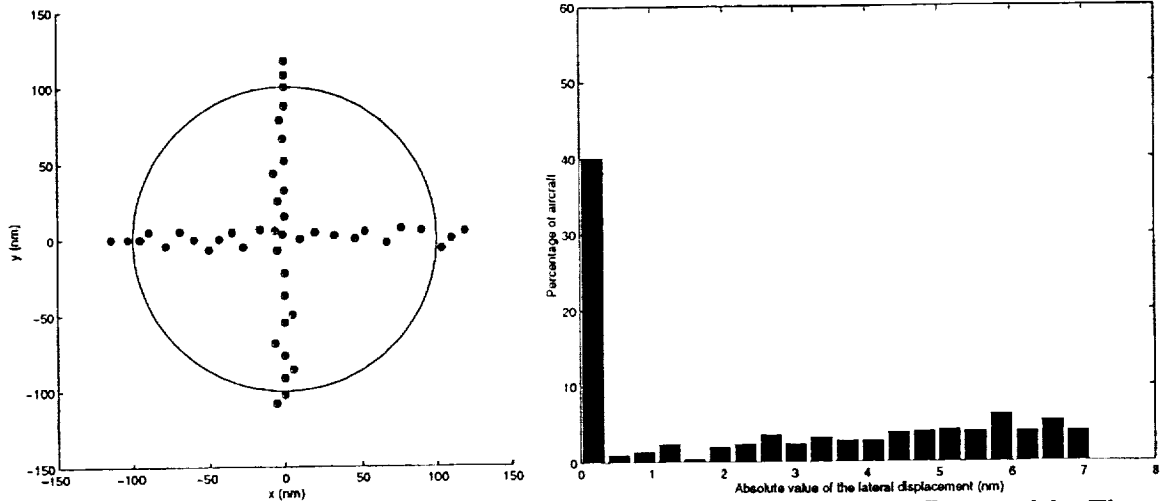
Figure 3-3: Test case for random arrival geometry using the lateral offset model. The separation distance is subject to a uniform distribution on the interval [5, 15] nm. The number of the tested aircraft is 500. Left: A snapshot taken during the conflict resolution process. Right: Aircraft deviation distribution.

take any action to avoid the conflict. Hence the conflict resolution is left to the eastbound aircraft only. It is easy to test that the minimum lateral displacement for the eastbound aircraft to avoid the conflict is exactly $\sqrt{2}d$. This example shows that the bound we obtained is tight. In general, it was observed that for the class of problems considered in this section, up to six aircraft can be involved in the same conflict.

3.2 Simulations

This section presents simulations of traffic under the conditions described above. The goal of the simulations is to estimate bounds on the maximum deviations actually experienced by the intersecting aircraft flows, as well as to generate some insight about the structure of the traffic flow after resolution. In this section, we will assume in the first two subsections that the aircraft resolve conflicts via lateral position changes. Some simulations for heading change maneuvers are given in the third subsection.

3.2.1 Random Arrival Geometry

We first examine the lateral displacement of aircraft in the two intersecting streams for random arrival patterns. The aircraft in either stream are initially separated
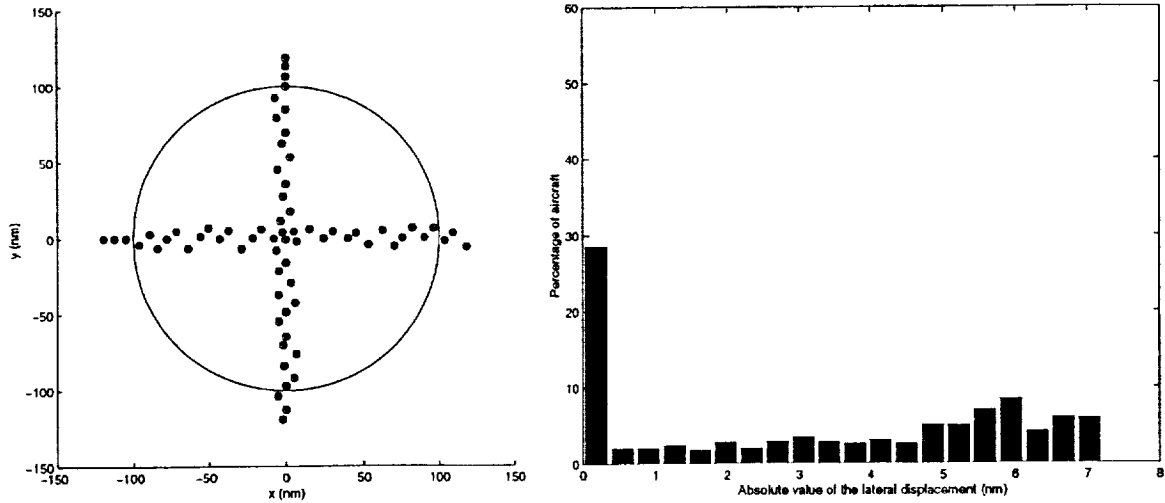
22

Figure 3-4: Test case for random arrival geometry using the lateral offset model. The separation distance is subject to a uniform distribution on the interval [5, 10] nm, and the number of the tested aircraft is 500. Left: A snapshot taken during the conflict resolution process. Right: Aircraft deviation distribution.

by a distance chosen from a uniform distribution over the interval [5, 15] nm. The considered airspace volume (conflict area) is circular with radius 100 nm. A total of 500 aircraft flowing through this airspace have been simulated. Fig. 3-3 gives a snapshot of the traffic flow taken during the conflict resolution process. Also shown in Fig. 3-3 is a histogram of the lateral deviations experienced by the 500 tested aircraft. The largest lateral displacement found in this simulation is 7.1 nm, which exactly is our estimated upper bound. The average of the lateral displacements of the tested aircraft is 2.68 nm, and there are 42.6% of the 500 tested aircraft deviating from the nominal path with a lateral displacement larger than half of the upper bound (approximately 3.5 nm).

Another simulation was run under the same conditions as above, except for the uniform distribution on the initial separation distance, which was changed from [5, 15] nm to [5, 10] nm. Fig. 3-4 gives the distribution plot and a snapshot taken during the conflict resolution process. In this simulation, the largest recorded lateral displacement is still 7.1 nm, and the average lateral displacement of the tested aircraft is 3.27 nm. There are 50.6% of the total aircraft deviating more than 3.5 nm. It can be seen that as the average density of the random aircraft flows increases, the possibility for an aircraft to experience a large lateral displacement increases consequently.

23
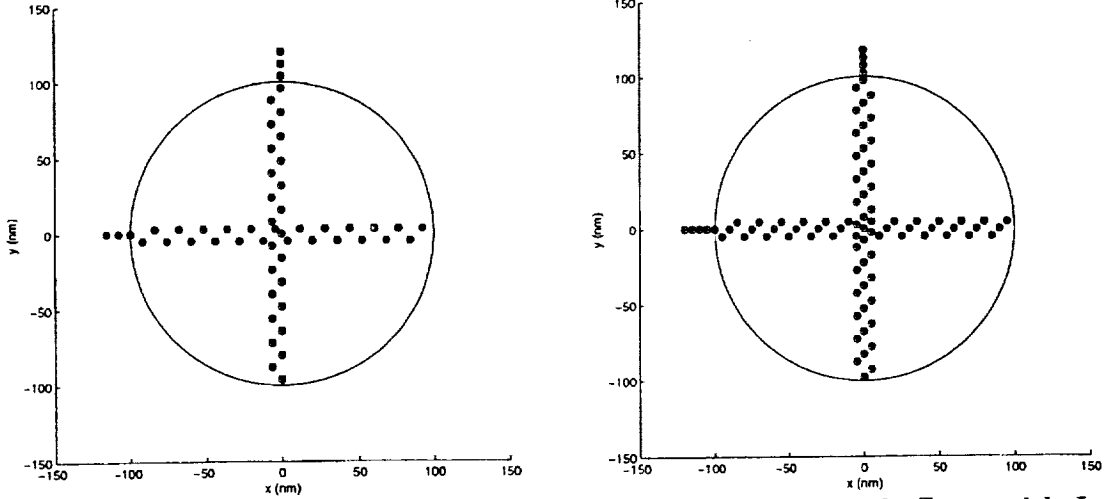
Figure 3-5: Test cases for uniform arrival geometry using the lateral offset model. Left: Separation distance is 8 nm. Right: Separation distance is 5 nm.

However, its deviations never exceed the estimated upper bound.

3.2.2 Uniform Arrival Geometry

The following simulations consider the conflict resolution for two streams of aircraft with fixed initial separation distance. Although this uniform aircraft arrival geometry is unrealistic, it may help us get some intuition, in addition to the stability analysis, about how the proposed avoidance rules can successfully handle the conflict resolution for two streams of aircraft.

Fig. 3-5 gives two examples. In the first example, the initial separation distance between every pair of neighboring aircraft is $S = 8$ nm. Denote $d_{s,0}$ as the initial distance between the first aircraft in the southbound stream and the center of the conflict area, and, correspondingly, denote $d_{e,0}$ for the first aircraft in the eastbound stream. In this example, $d_{s,0}$ and $d_{e,0}$ are chosen such that $d_{s,0} - d_{e,0} = S/2$. Thus aircraft enter into the control volume one at a time. Fig. 3-5 (left picture) shows the structure of the traffic flow after conflict resolution. The largest lateral displacement experienced by the aircraft is 6.2 nm. In the second example, we chose the initial separation distance of aircraft to be $S = d = 5$ nm, and $d_{s,0} - d_{e,0}$ to be $S/2$. In this case the aircraft are "packed" in the most compact way before they flow into the conflict area. Fig. 3-5 (right picture) shows a snapshot of the flows for this case

24
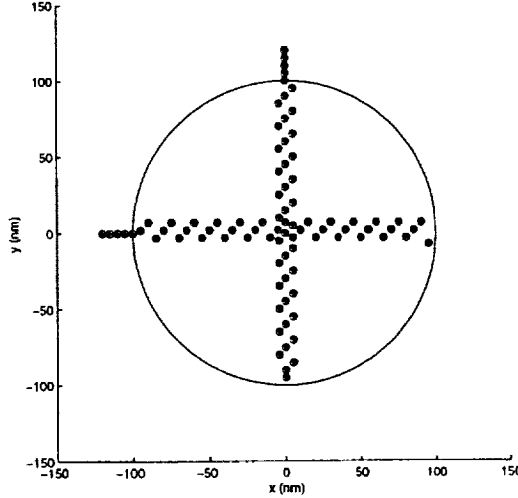
Figure 3-6: Test case for uniform and simultaneous arrival geometry using the lateral offset model.

during the conflict resolution process. The largest lateral displacement of the aircraft is 5 nm. The displacements for both examples are within our estimated upper bound. However, these examples show that aircraft deviation amplitude is not necessarily monotonic with flow density.

From the above two examples we also observe that uniform aircraft arrival flows generate periodic, conflict-free aircraft flow patterns under the simple conflict avoidance rule. Furthermore, the conflict avoidance rule groups the aircraft in "platoons", and each platoon is formed in such a manner that the aircraft in a platoon have the same "shadow" as that of other aircraft in the same platoon. Intuitively, this kind of platooning is very efficient for conflict resolution involving two aircraft flows. The platooning results in a "shearing" motion when two platoons (from the two aircraft streams) meet at the center of the conflict area. Interesting enough, platooning has been proposed as a viable, although heuristic option in many intelligent, hierarchical transportation systems [40, 9].

Next, considering closely spaced flows ($S = 5$), we determined the behavior of the flows as $d_{s,0} - d_{e,0}$ decreases to 0, that is, eastbound and southbound aircraft enter the control volume nearly at the same time. Fig. 3-6 presents a snapshot of the flows for this case during the conflict resolution process. It is observed that the platooning pattern does not change. The largest lateral displacement of the aircraft is 7.1 nm.

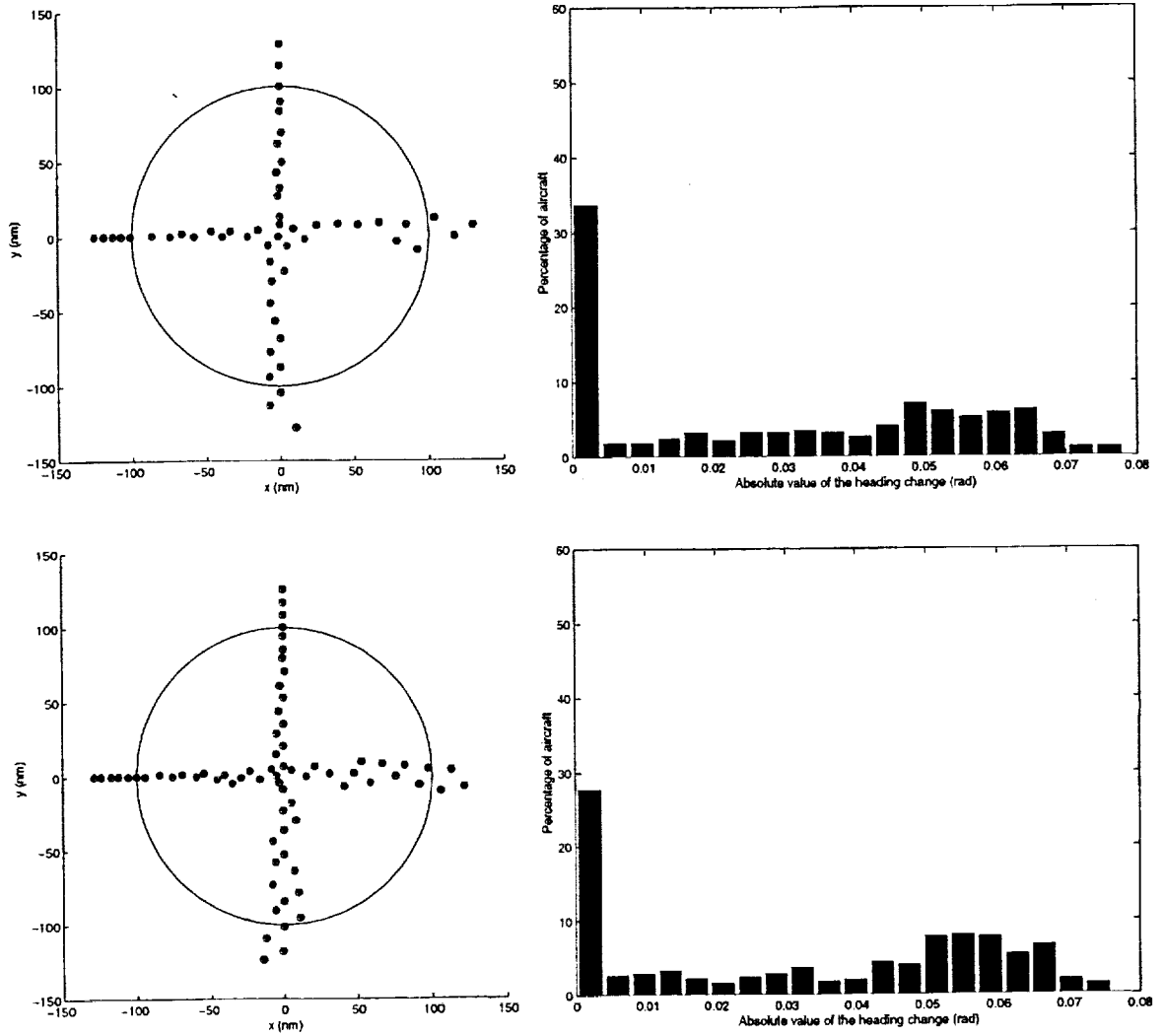Figure 3-7: Test cases for random arrival geometry using the heading control model. The separation distance of aircraft is subject to a uniform distribution on the interval $[5, 15]$ nm for the upper test case, and $[5, 10]$ nm for the lower test case. The number of the tested aircraft is 500 in both cases. Left: Snapshots taken during the conflict resolution process. Right: Aircraft deviation distributions.
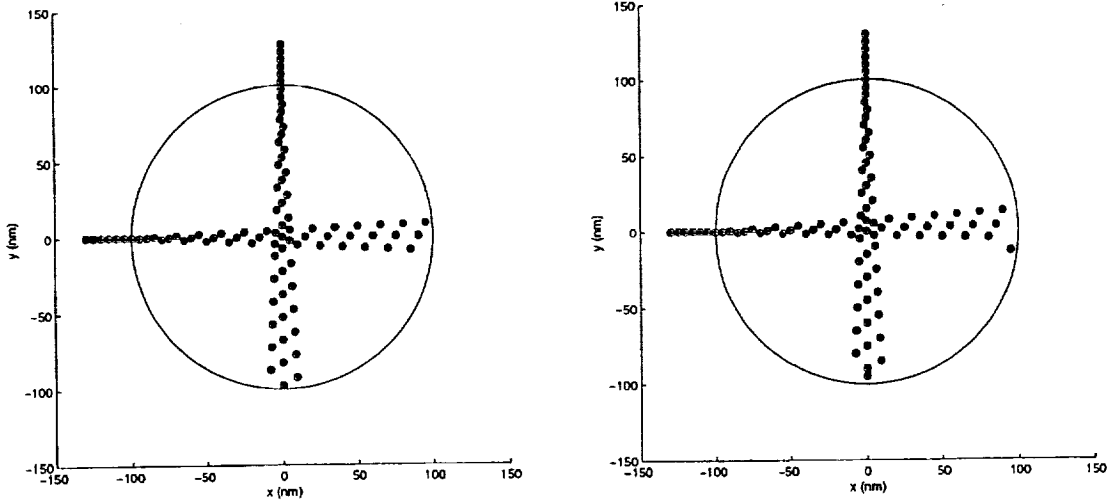
Figure 3-8: Test cases for uniform arrival geometry using the heading control model. In both cases, the separation distance is 5 nm, and the radius of the conflict area is 100 nm. Left: In-turn arrival pattern. Right: Simultaneous arrival pattern.

3.2.3 Stability Results for Heading Control Model

As mentioned in the previous sections, the lateral offset model may be considered as an approximation to the heading control model. The approximation accuracy can be examined by comparing the reachable position sets (areas) of both models for a given time horizon interval $[T, T + \Delta T]$. In this subsection, we use the following four simulations to illustrate the similarity between the two models.

The first two simulations are run under the same conditions as described in the simulations of Fig. 3-3 and Fig. 3-4. The left pictures in Fig. 3-7 give snapshots taken during the conflict resolution process, while the right pictures in Fig. 3-7 show the distributions of the tested aircraft with respect to their heading changes. There is significant similarity between the distributions in Figs. 3-3, 3-4 and Fig. 3-7. Note that a heading change of 0.01 radian results in approximately a lateral displacement of 1 nm lateral displacement after the aircraft flies 100 nm straight.

The third and fourth simulations use the heading change model to resolve conflicts for scenarios with uniform arrival geometry. In these two examples, the initial separation distances of aircraft are $S = 5$ nm, while $d_{s,0} - d_{e,0}$ are $S/2$ and 0 respectively. Fig. 3-8 shows the structures of the resulting traffic flow, which are similar to those observed in Fig. 3-5 (right picture) and Fig. 3-6. Note that in the these

two simulations we ignore the slight "jostling" which may possibly occur between two neighboring aircraft.

From the examples presented above, we see that the lateral offset model appears to be a good approximation to the heading control model, especially for very small perturbations.

3.2.4 Discussion

The simplicity of the stability analysis stands with no doubt in contrast with the complexity of the observed aircraft behaviors during simulations: While aircraft conflict avoidance behaviors may display a large number of possible behaviors, it is possible to determine an upper bound on the lateral deviation by using first principles. The case study performed here reveals that crucial to the proof of flow stability is the fact that vehicles behave "intelligently" as they attempt to minimize the deviation from their intended path. It is worth noting that statistical approaches such as the one presented in [35], for example, because they perform open-loop analyses, would have resulted in a very large number of predicted conflicts. In comparison, the present analysis, because it is performed on the *closed-loop* system, predicts no conflict will ever occur and the traffic flow will be handled efficiently (deviations remain bounded). On the other hand, the current analysis pays no attention to robustness issues and what happens in case of delinquent aircraft behavior. Such analysis is the object of future research.

3.3 Generalizations

This section makes several generalizations to the basic conflict scenario of two aircraft flows. In this section, we assume that the aircraft resolve conflicts via lateral position changes.

28
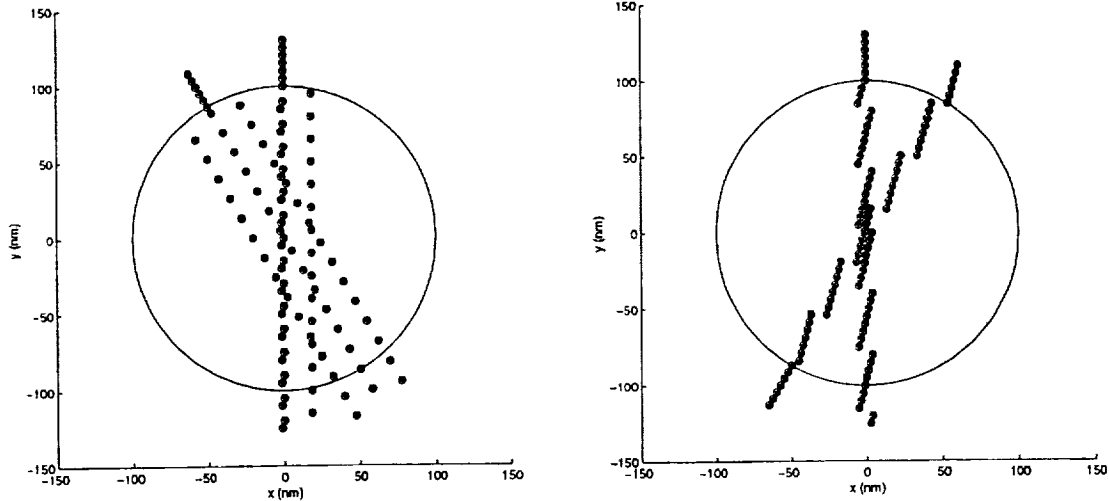
Figure 3-9: Test cases for two aircraft flows with different encounter angles. Left: Encounter angle is 30 deg. Right: Encounter angle is 150 deg.

3.3.1 Arbitrary Encounter Angles

Let θ be the encounter angle between aircraft flows: $\theta = 0$ deg corresponds to the case when the two flows are parallel and $\theta = 180$ deg corresponds to the two flows going opposite directions.

A slight generalization of the previous reasoning allows us to prove that for arbitrary flow encounter angles, the lateral deviation of each aircraft is bounded above by

$$\frac{d}{|\sin(\theta/2)|}. \tag{3.2}$$

Detailed proof for a generalized version of (3.2) can be found in Section 3.3.4.

Two simulations with different encounter angles of the two aircraft flows are shown in Fig. 3-9. The aircraft streams in both simulations have fixed initial separation distance, $S = d = 5$ nm. The largest lateral displacements of aircraft in the two examples are 19.3 nm and 5.2 nm respectively, exactly the same as the bounds obtained by (3.2). Note that the lateral displacement of aircraft could be very large when the encounter angle is small. It is also observed that when θ approaches 180 deg, there could be a large number of aircraft involved in the same conflict. In the example presented in Fig. 3-9 (right picture), the maximum number of aircraft involved in the same conflict is 16, while this number is 6 for the case of $\theta = 90$ deg.

29
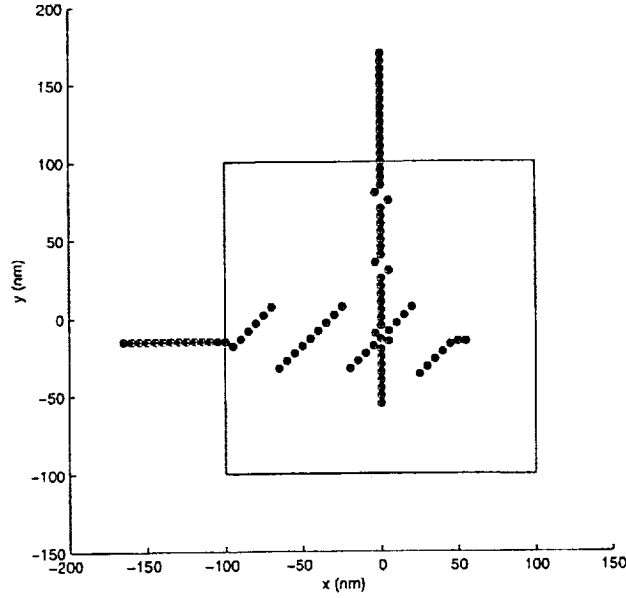
Figure 3-10: Two aircraft streams maneuvering at different times to conflict.

3.3.2 Aircraft Maneuvering at Different Times to Conflict

The *time to conflict* is defined as the period of time that is needed by an aircraft to fly, at the original velocity before resolution, from the point where the aircraft enters the control volume to the conflicting point, *i.e.*, the intersection point of the aircraft nominal paths. In the above definition, the distance between the point where an aircraft enters the control volume and the conflicting point is called the *distance to conflict*.

In our previous discussions, the control volume is assumed to be circular. However, our proof of stability has no specific requirement on the shape of the control volume. The control volume only needs to satisfy that each aircraft entering the control volume maneuvers at the same time to conflict.

This subsection will discuss the situation where the aircraft maneuver at different times to conflict. Consider two crossing aircraft flows, one eastbound and the other southbound. All aircraft fly at the same speed. Let d_1 and d_2 be the distances to conflict for the eastbound aircraft and southbound aircraft, respectively. If $d_1 \neq d_2$, then the eastbound aircraft and southbound aircraft maneuver at different times to conflict. Without loss of generality, assume $d_1 \leq d_2$.

Following the similar steps as given in the stability proof of Section 3.1, we can

derive that, in the conflict resolution for the above scenario, the lateral deviation of each eastbound aircraft is bounded by

$$\sqrt{2}d + |d_1 - d_2|, \qquad (3.3)$$

and the lateral displacement of each southbound aircraft is bounded by

$$\sqrt{2}d. \qquad (3.4)$$

This conclusion can also be treated as a corollary of the result in Section 3.3.4, where a detailed proof is given.

Fig. 3-10 shows a test example, in which the control volume is a square with $d_1 = 100$ nm and $d_2 = 115$ nm. The aircraft streams in this simulation have fixed initial separation distance, $S = d = 5$ nm. The largest lateral displacement is 22.1 nm for the eastbound aircraft, and is 5 nm for the southbound aircraft, both of which are within the bounds obtained by (3.3) and (3.4). Also we could notice that the aircraft responding later to a conflict will on average experience larger lateral deviation to resolve the conflict.

3.3.3 Two Streams of Aircraft with Different Speeds

This subsection relaxes the assumption of "same aircraft speed" to "different aircraft speeds". Let v_1 and v_2 be the speeds of aircraft in the two streams, respectively, and denote $\mu = v_2/v_1$. For simplicity, we assume the encounter angle between the two aircraft flows is 90 deg, and in order to be fair to the aircraft in different streams, we assume that each aircraft maneuvers at the same time to conflict. (These two assumptions will be relaxed in the next subsection.) Therefore we have $d_2 = \mu d_1$, where d_i is the distance to conflict for aircraft with speed v_i, $i = 1$ or 2.

Denote θ_i as the angle between the aisle and the flying direction of the aircraft with speed v_i, $i = 1$ or 2. It can be tested that $\theta_1 = \cos^{-1}(\frac{1}{\sqrt{1+\mu^2}})$ and $\theta_2 = \cos^{-1}(\frac{\mu}{\sqrt{1+\mu^2}})$. Then we can derive that, in the conflict resolution for the above scenario, the lateral

31
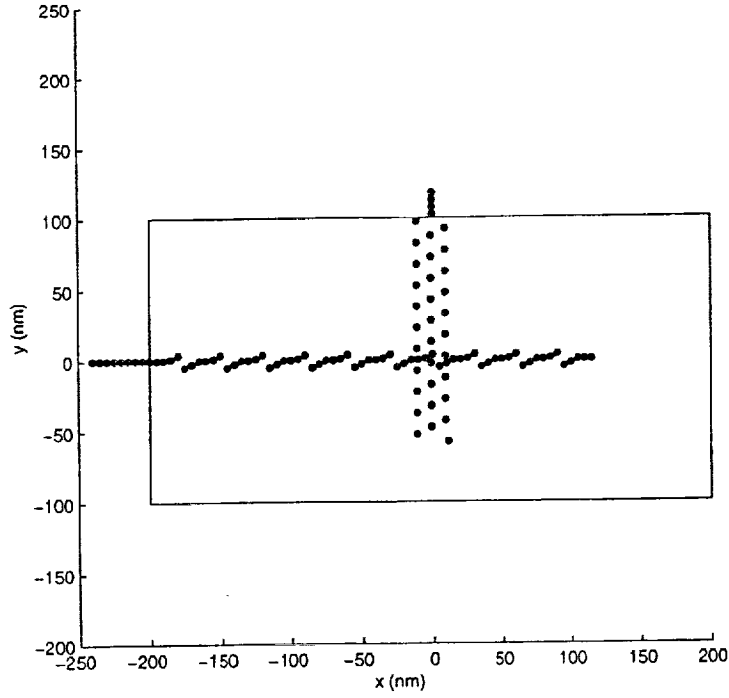
Figure 3-11: Two aircraft streams with different speeds (ratio 2 : 1), but maneuvering at the same time to conflict.

deviation of aircraft with speed v_1 is bounded by

$$d\sqrt{1+\mu^2}, \tag{3.5}$$

and the lateral deviation of aircraft with speed v_2 is bounded by

$$\frac{d\sqrt{1+\mu^2}}{\mu.} \tag{3.6}$$

Fig. 3-11 gives a test example for two streams of aircraft with speed ratio 2 : 1.

3.3.4 Existence of Conflict Resolution for General Encounter Patterns

In this subsection, we analyze the system performance of the two aircraft flows, taking into account all the generalizations we made previously: The two flows of aircraft considered here may have arbitrary encounter angles, different times to conflict and different speeds.

Consider two aircraft streams, stream 1 and stream 2. Let v_1 and v_2 be the speeds

of aircraft in stream 1 and stream 2 respectively, and denote $\mu = v_2/v_1$. Let θ be the encounter angle between the two aircraft streams. Denote d_i as the distance to conflict for the aircraft in stream i, and let θ_i be the angle between the aisle (or the relative velocity vector) and the flying direction of the aircraft with speed v_i, $i = 1$ or 2. Without loss of generality, we consider a conflict scenario as shown in Fig. 3-12, in which the axes are chosen such that the aircraft in stream 1 are originally located on the x axis, flying towards the positive direction of x axis, and the original tracks of the two aircraft streams intersect at the origin. In Fig. 3-12, the aircraft to perform the resolution is from stream 1, and is indicated in bold.

An estimate of the performance bound for the above system is presented in the following theorem. Without loss of generality, the estimate is given for the aircraft from stream 1. (The estimate for stream 2 is just a matter of changing notation indices correspondingly.)

Theorem 3.1: θ_1 is determined by

$$\cos^{-1}\left(\frac{1 - \mu \cos\theta}{\sqrt{1 + \mu^2 - 2\mu \cos\theta}}\right). \tag{3.7}$$

If $\mu = \frac{1}{\cos\theta}$ or $\mu = \cos\theta$, the aircraft from stream 1 or stream 2 can not resolve potential conflicts via lateral position changes only. If $\mu \neq \frac{1}{\cos\theta}$ and $\mu \neq \cos\theta$, the aircraft with speed v_1 can always execute a lateral displacement maneuver that results in a conflict-free trajectory. Further, the lateral displacement is bounded above by

$$\frac{d}{|\cos\theta_1|} + \max\{d_2 \sin\theta + d_2 \cos\theta \tan\theta_1 - d_1 \tan\theta_1, 0\} \tag{3.8}$$

Proof: It is not difficult to obtain the expression for θ_1 through checking the relations among the edges and angles of a triangle. We skip over the details.

If $\mu = 1/\cos\theta$ or $\mu = \cos\theta$, $\cos\theta_1$ or $\cos\theta_2$ will be equal to 0. That is to say the aisles of aircraft in stream 1 or stream 2 will be perpendicular to the flying direction of the aircraft. Thus, the aircraft from stream 1 or stream 2 can not resolve conflicts
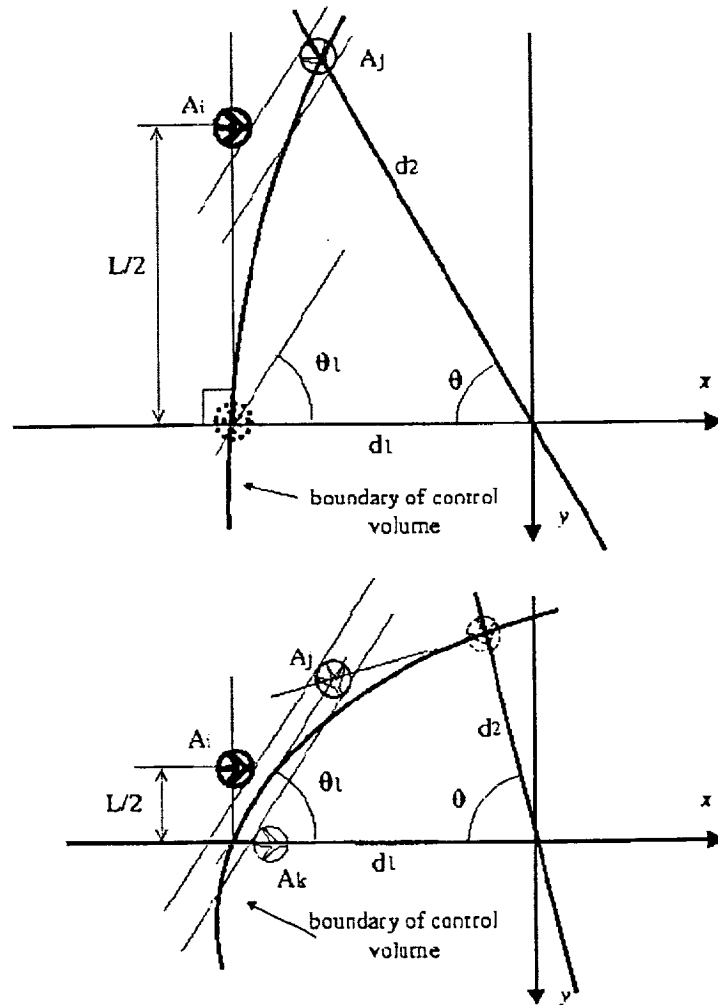
33

Figure 3-12: Existence of conflict resolution maneuver under general encounter patterns. Upper: The case of $d_1/v_1 \leq d_2/v_2$. Lower: The case of $d_1/v_1 > d_2/v_2$,

via lateral position changes only.

Assume $\mu \neq 1/\cos\theta$ and $\mu \neq \cos\theta$. Then there are two possibilities for θ_1: $\cos\theta_1 > 0$ or $\cos\theta_1 < 0$. Note that the arguments for these two situations are similar to each other. Without loss of generality, we only consider the case of $\cos\theta_1 > 0$ in the rest of this proof.

We will show that the aircraft entering the control volume (bold in Fig. 3-12) can always execute a lateral offset maneuver that results in a conflict-free trajectory, if L, the width of the maneuver corridor, is sufficiently large. As in the stability proof of Section 3.1, we start with the hypothesis that such a maneuver does *not* exist, and then consider the following two cases.

Case 1: $d_1/v_1 \leq d_2/v_2$. In other words, the aircraft in stream 1 respond to conflicts no earlier than the aircraft in stream 2. It can be tested that $d_1/v_1 \leq d_2/v_2$ is equivalent to

$$d_2 \sin\theta + d_2 \cos\theta \tan\theta_1 \geq d_1 \tan\theta_1.$$

Please refer to Fig. 3-12 (upper picture).

Under the hypothesis we made previously, there should be no aircraft from stream 1 in the following region:

$$\{(x, y) \mid -L/2 \leq y + \tan\theta_1 (x + d_1) \leq L/2\}. \tag{3.9}$$

Otherwise, the aircraft in bold (denoted by A_i) could hide behind such aircraft (from stream 1) in region (3.9), and therefore, succeed in finding a lateral displacement (no greater than $L/2$) that results in a conflict-free trajectory.

At the same time, all maneuvered aircraft from stream 2 have already performed minimum lateral displacement conflict resolution maneuvers. By hypothesis, their aisles intersect the protected circle of A_i, wherever its location is, since no conflict resolution is possible. Especially, at least one aisle intersects the protected circle A_i when A_i deviates fully to the left, as shown in Fig. 3-12 (upper picture).

For aircraft A_i to deviate fully to the left of the maneuver corridor, the location

35

(x_j, y_j) of the corresponding aircraft from stream 2 (denoted by A_j) must satisfy

$$y_j + \tan\theta_1 (x_j + d_1) \leq -L/2 + d/|\cos\theta_1|. \tag{3.10}$$

Assume

$$L/2 > \frac{d}{|\cos\theta_1|} + d_2 \sin\theta + d_2 \cos\theta \tan\theta_1 - d_1 \tan\theta_1. \tag{3.11}$$

This assumption implies that aircraft A_j is inside region (3.9). From the above argument about region (3.9), we see that aircraft A_j need not make any lateral displacement maneuver for conflict avoidance, because there is no aircraft from stream 1 inside this region. Therefore, the location (x_j, y_j) of A_j should stay on the nominal path of stream 2, with a distance to the origin no greater than d_2. Thus, we have

$$y_j + \tan\theta_1\, x_j \geq -d_2 \sin\theta - \tan\theta_1 (d_2 \cos\theta). \tag{3.12}$$

From (3.10) and (3.12), we may derive

$$L/2 \leq \frac{d}{|\cos\theta_1|} + d_2 \sin\theta + d_2 \cos\theta \tan\theta_1 - d_1 \tan\theta_1, \tag{3.13}$$

which causes contradiction with assumption (3.11).

Case 2: $d_1/v_1 > d_2/v_2$, which is equivalent to

$$d_2 \sin\theta + d_2 \cos\theta \tan\theta_1 < d_1 \tan\theta_1.$$

Please refer to Fig. 3-12 (lower picture).

Similar to the argument in Case 1, we see that there should be no aircraft from stream 1 in the region of (3.9), and there must be at least one aircraft from stream 2, say A_j, whose aisle intersects the protected circle A_i when A_i deviates fully to the left (in the maneuver corridor). Thus the location (x_j, y_j) of A_j satisfies (3.10).

Because $d_2 \sin\theta + d_2 \cos\theta \tan\theta_1 < d_1 \tan\theta_1$, we may induce that it is needed of aircraft A_j to make a nonzero lateral displacement maneuver for conflict resolution. For this to happen, there must exist an aircraft from stream 1, say A_k, whose aisle

intersects the aisle of A_j on the other side of A_j opposite to A_i. Therefore, (x_k, y_k), the location of aircraft A_k, should satisfy

$$y_k + \tan \theta_1 \, x_k = y_j + \tan \theta_1 \, x_j + d/|\cos \theta_1|. \qquad (3.14)$$

According to (3.10), we have

$$y_k + \tan \theta_1 \, x_k \leq -L/2 - \tan \theta_1 \, d_1 + 2d/|\cos \theta_1|. \qquad (3.15)$$

Further, since A_k is not included in region (3.9) and is on the other side of region (3.9) opposite to A_i, we have

$$y_k + \tan \theta_1 \, x_k \geq L/2 - \tan \theta_1 \, d_1. \qquad (3.16)$$

Assume

$$L/2 > d/|\cos \theta_1|. \qquad (3.17)$$

It is easy to test that under such assumption, (3.15) and (3.16) are contradictory with each other. Therefore, there must exist a conflict avoidance maneuver for A_i with

$$L/2 \leq d/|\cos \theta_1|. \qquad (3.18)$$

The arguments in Case 1 and Case 2 have shown the existence of the conflict avoidance maneuver. The largest displacement of aircraft is bounded above by (3.13) when $d_2 \sin \theta + d_2 \cos \theta \tan \theta_1 \geq d_1 \tan \theta_1$, and by (3.18) when $d_2 \sin \theta + d_2 \cos \theta \tan \theta_1 < d_1 \tan \theta_1$. Equivalently, the largest displacement of aircraft is bounded by (3.8). Q.E.D.

It is easy to test that the conclusions of Sections 3.3.1-3 are just special cases of Theorem 3.1: (1) When $v_1 = v_2$ and $d_1 = d_2$, (3.8) becomes (3.2), the performance estimate for arbitrary encounter angles; (2) Under conditions of $\theta = 90$ deg and $v_1 = v_2$, (3.8) is equivalent to (3.3) and (3.4); For the case of $d_1/v_1 = d_2/v_2$ and

$\theta = 90$ deg, Theorem 3.1 reveals the same conclusion as obtained in Section 3.3.3.

3.3.5 Multiple Aircraft Flow Streams

The conflict resolution for two aircraft streams has been investigated in the previous sections. The theoretical arguments and the simulation experiments have shown it is possible to quantify the efficiency and stability of the simple decentralized conflict avoidance rules used in two aircraft flow streams. We now address the following question: What happens when multiple (more than two) aircraft flow streams are involved? This question is being investigated using numerical simulations, and the results indicate this problem might be considerably more difficult to investigate than that involving two aircraft flows only.

Consider three streams of aircraft, initially uniformly separated by the distance $S = 10$ nm. (The total arriving rate of aircraft in this three streams is smaller than that of the two stream aircraft problem with separation distance $S = 5$ nm.) The three crossing aircraft flows are oriented 120 degrees with respect to each other. The conflict area is a circle centered at the intersecting point of the nominal paths of the three streams. The radius of the circle is 150 nm. It is assumed that aircraft from each flow enter the conflict area simultaneously and that the same decentralized conflict resolution is applied with priority given first to the northeast-bound aircraft (stream 1), then to the northwest-bound aircraft (stream 2) and finally to the southbound aircraft (stream 3).

An illustration of the conflict resolution geometry and a time history of the lateral displacements experienced by the first 240 aircraft is given in Fig. 3-13. Note that, in order to identify easily the aircraft from different streams in the snapshot of the resolution, we use different symbols to represent the aircraft from different streams.

The largest displacement experienced by the first 240 tested aircraft is 34.6 nm. Although the aircraft flow has uniform arrival geometry, the resulting flow is very complex and shows large deviations from the nominal path; this flow exhibits no apparent periodicity in the resolution maneuver amplitude.

Let us look at another example of three aircraft flows, in which the conflict reso-

lution even does not exist. Please refer to Fig. 3-14. The initial separation distance of aircraft is $S = 5$ nm, and the aircraft from each stream enter the conflict area simultaneously. We can prove for this example that the lateral displacement of the aircraft (except the first one) in each stream will linearly increase as the aircraft number increases. Therefore, under the decentralized conflict avoidance rules and the lateral offset maneuver model, there will be no resolution for this three aircraft flow problem. Fig. 3-14 presents a snapshot of the conflict resolution and a time history of the lateral displacements experienced by the first 105 aircraft (35 in each stream).

Compared with two aircraft flows, three aircraft flow scenarios are much more difficult to handle. This comes into being not only because of the possible increase in the aircraft density inside the conflict area, but also because the heading change maneuver or the lateral position change maneuver can not provide efficient platooning patterns for three aircraft flows. In the case of two aircraft streams, it is possible for the aircraft to organize platoons using the proposed conflict avoidance rules. The platoons have the property that from the view point of the aircraft in the other stream, the aircraft in a platoon can hide behind the shadows (aisles) of the aircraft in the same platoon. However, this is no longer true for three aircraft flows. Intuitively, for more dispersed aircraft streams, it is difficult for an aircraft in one stream to hide in the shadow of another aircraft in the same stream, because the conflicting aircraft may be coming from more than one direction.
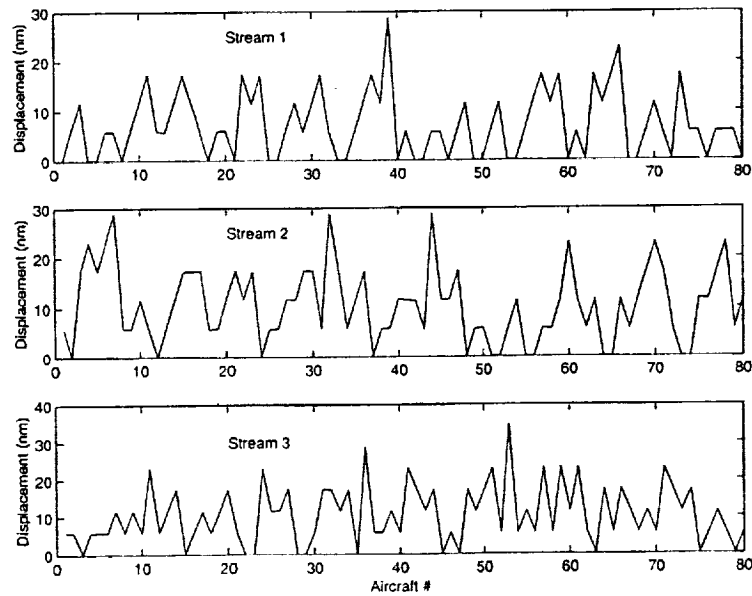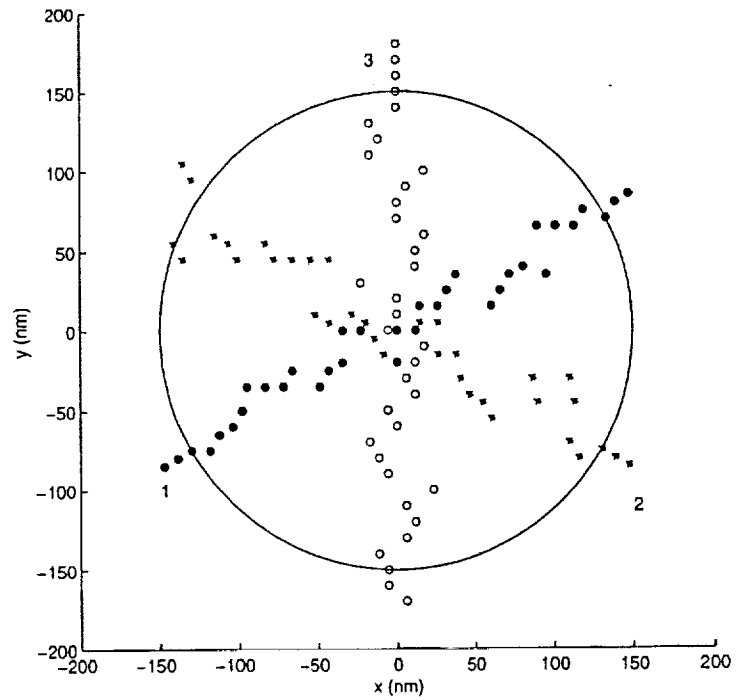
Figure 3-13: Upper: Test case for three aircraft flows with uniform and simultaneous arrival geometry using the lateral offset model. The initial separation distance is 10 nm. The largest displacement experienced by the tested 240 aircraft is 34.6 nm. In the plot, we use different symbols to represent the aircraft from different streams. Lower: Deviation histogram for three aircraft flow streams.

40
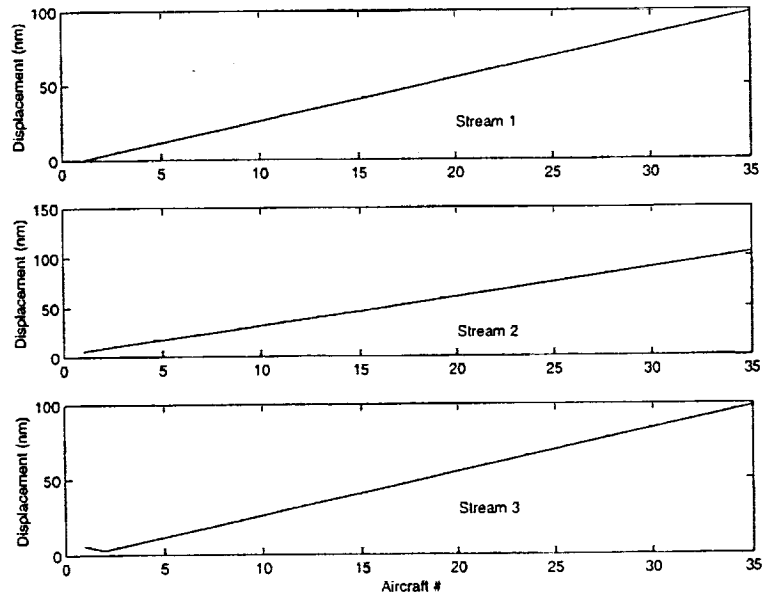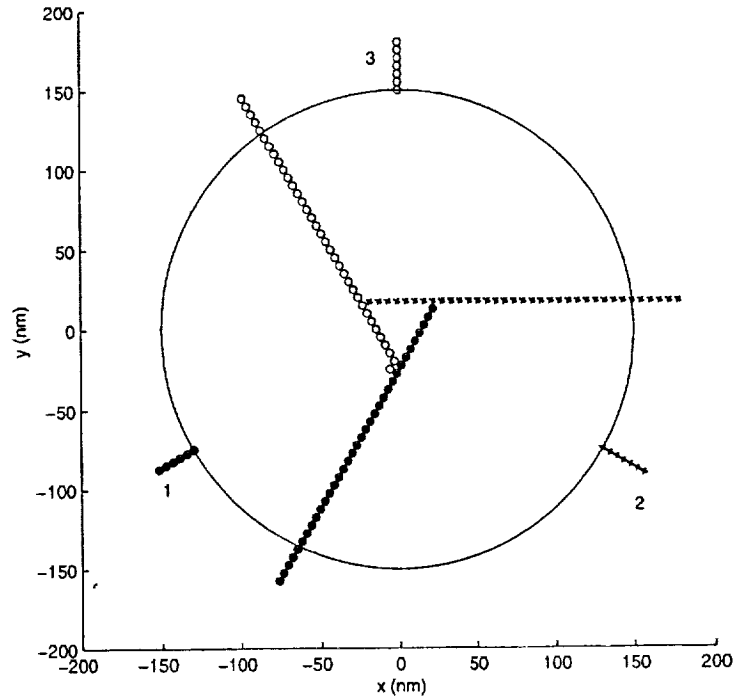
Figure 3-14: Upper: Test case for three aircraft flows with uniform and simultaneous arrival geometry using the lateral offset model. The initial separation distance is 5 nm. The largest lateral displacement experienced by the first 60 aircraft is 60.7 nm. In the plot, we use different symbols to represent the aircraft from different streams. There is no resolution for the whole system (with infinite number of aircraft in each stream).

Chapter 4

Aircraft Flow Stability under Offset Model and Velocity Change Model

This chapter builds upon the developments of Chapter 3 by expanding the range of allowable aircraft behaviors from lateral position change to general position change, and from heading control only to both speed and heading control. As mentioned previously, the offset model can be viewed as an approximate model of the velocity change model, and takes the advantage of its simplicity for analysis purposes. In this chapter, the theoretical analysis, including the proofs of existence of conflict resolution maneuvers and the estimates of performance bounds, will be concentrated on the offset model, while simulation examples are designed and run for both the offset model and velocity change model.

In comparison with Chapter 3, this chapter considers the aircraft modeled with more control freedom in the conflict resolution. We notice that the increase of freedom of individual aircraft may possibly bring about "greedy" decision making for such aircraft. As a consequence, the maneuvering aircraft may possibly leave serious conflicting situations to the aircraft that have not yet maneuvered. Will this yield instability of the whole system? That is the question we are about to answer in this chapter.

4.1 A Special Type of Penalty Functions and System Stability

4.1.1 Penalty Functions

We assume in the offset model each aircraft attempts to minimize the "amplitude" or *penalty function* of the required relative position deviation while remaining within prescribed lateral and longitudinal bounds. Each aircraft may use a different penalty function to reflect pilot preferences. And the aircraft may use different weights on the lateral position displacement and the longitudinal position displacement in their penalty functions due to the consideration of physical limitations of the aircraft or specific conflict conditions, *etc.*

In fact, the lateral offset model can be treated as an offset model with the choice of penalty functions revealing that the longitudinal deviation is much more costly than the lateral deviation.

In this section, we assume that each aircraft attempts to minimize the amplitude of its lateral deviation, irrespective of the amplitude of its longitudinal displacement, under the premise that the largest backward and forward displacements of each aircraft, b and f, are restricted to be no greater than a fixed value. According to this assumption, the aircraft use the penalty functions which put much "heavier" weight on the lateral displacements than on the longitudinal displacements. We know that the lateral displacements of the aircraft in a stream determine the size of the "maneuver corridor". The smaller the corridor size is, the less airspace we need to reserve for the conflict resolution, and the more free airspace there is available for handling other air traffic. With such concern, we emphasize on minimizing the lateral displacements of aircraft in this section.

However, we should be noted that this choice of penalty functions is not very realistic. It is intended with more concern as an exercise aimed at comparing with what happens in the more realistic case when general penalty functions are being used. Discussions for offset model with general penalty functions will be given in the

third section of this chapter.

4.1.2 Conflict Geometry

For simplicity, we assume that the two crossing aircraft flows with same speed are oriented 90 degrees with respect to each other, as shown in Fig. 3-1. (These assumptions may be relaxed to general situations like those in Section 3.3.) And we assume that aircraft resolve conflicts via lateral and longitudinal position changes.

Considering lateral and longitudinal position change maneuvers, an aircraft not only needs to consider the possible conflict with the aircraft in the other aircraft stream, it should also take into account the possible conflict with the aircraft in the same stream. Physical considerations made earlier indicate that physically significant longitudinal aircraft maneuvers may not exceed 5 nm over a 10 min time horizon to conflict. Thus we will assume in this chapter that the largest backward and forward displacements of each aircraft (b and f) are no greater than the safety distance d (usually 5 nm).

Based on the assumptions for the conflict resolution rules, an aircraft solving a conflict does not consider the potential conflicts with the aircraft that have not yet maneuvered. Therefore, when an aircraft is relatively moving backward, it may possibly "jostle" the following aircraft before that aircraft enters the control volume. However, we know that the position change (offset) maneuvers can not be performed instantaneously, because they must be realized by velocity changes and must be the effect of the integration of velocity deviations over a period time. Thus the maneuvering aircraft could at most jostle the following aircraft to a very small extent before the following aircraft maneuvers to avoid conflicts. We ignore such slight jostling in the offset model.

4.1.3 Existence of Conflict Resolution Maneuver

We will show that, if the width of the maneuver corridor, L, is large enough, any aircraft entering the control volume can always execute an offset maneuver that results

44

Figure 4-1: Existence of conflict resolution maneuver.

in a conflict-free trajectory. We proceed with the proof by contradiction. First, assume that such a conflict-free maneuver does not exist.

The aisles of the eastbound aircraft ahead of E_i should not cover the protected circle of E_i, wherever E_i is located within its "reachable area". Otherwise, aircraft E_i could safely hide behind one of these aisles. Hence, there should not exist any aircraft other than E_i in the shaded area shown in Fig. 4-1. This area is the sum of the area P that is reachable by aircraft E_i after maneuvering, the right triangle S whose hypotenuse is inclined 45 degrees, minus the trapezoid T, whose dimensions are shown in the picture. It is easy to see that if there exists any eastbound aircraft E_k (other than E_i) located in the area $P + S - T$, then aircraft E_i could arrange a position change such that it is able to hide behind E_k to avoid conflicts from the southbound aircraft.

The maneuvered southbound aircraft must have performed conflict resolution maneuvers with minimum lateral displacement. Their aisles should intersect the protected circle E_i, wherever its location is, since no conflict resolution is possible for aircraft E_i. At least one aisle must intersect the protected circle E_i when E_i deviates backwards with amplitude d and to the left with amplitude $L/2$, as shown in Fig. 4-1.

Assume

$$L > 2\sqrt{2}d. \tag{4.1}$$

45

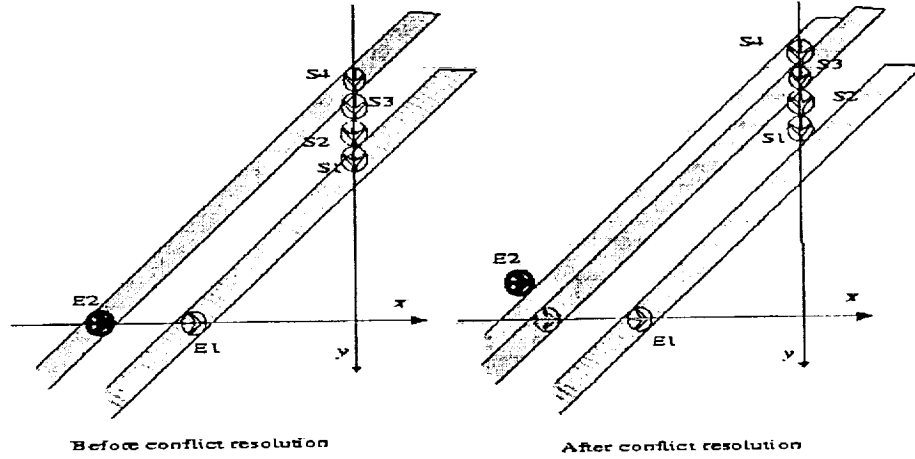Before conflict resolution   After conflict resolution

Figure 4-2: A constructed example showing that the estimated bound is tight.

Since the aisle of S_l should overlap the protected circle of E_i when E_i deviates fully backwards and to the left with amplitude $L/2$, S_l must have deviated backwards with amplitude d and have deviated to the right (from its nominal path) by a distance larger than $L/2 - \sqrt{2}d > 0$. However, from the optimality assumption on the maneuver of S_l, S_l need not deviate sideways after deviating fully backwards, because after the backward offset maneuver S_l would have had no conflict with any maneuvered southbound aircraft and eastbound aircraft (note that there is no eastbound aircraft in the shaded area of $P + S - T$ in Fig. 4-1). Thus we reach a contradiction. Hence there must exist a conflict avoidance maneuver for E_i with lateral displacement not greater than $\sqrt{2}d$, and the closed-loop system is therefore stable.

We now show the bound on the maximum lateral displacement, $\sqrt{2}d$, is tight. Fig. 4-2 constructs an example in which the aircraft in bold must make a position change with the lateral displacement amplitude $\sqrt{2}d$ to resolve the conflict. In this example, we assume that for all aircraft $b = f = d$. If two aircraft enter the control volume simultaneously, the southbound aircraft is assumed to maneuver first. Assume 4 southbound aircraft and 2 eastbound aircraft enter the control volume. Let R be the radius of the control volume. The initial positions of the southbound aircraft are $(0, -R - id)$, $i = 1, 2, 3, 4$, and the two eastbound aircraft's positions in the (x, y) coordinate system shown are $(-R - 2d + \sqrt{2}d, 0)$ and $(-R - 4d, 0)$ respectively. It can be seen the resulting aircraft behavior under conflict resolution is as follows: The first
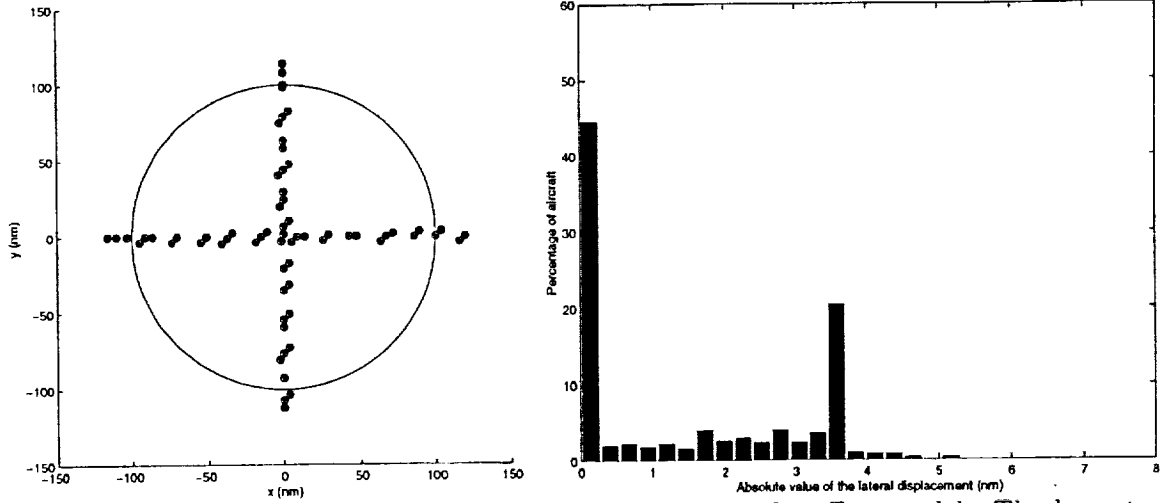
46

Figure 4-3: Test case for random arrival geometry using the offset model. The largest backward and forward displacements are restricted to be 5 nm. The initial separation distance is subject to a uniform distribution on the interval [5, 10] nm, and the number of the tested aircraft is 500. Left: A snapshot taken during the conflict resolution process. Right: Aircraft deviation distribution.

eastbound aircraft need not maneuver; Each of the southbound aircraft will undergo a backward longitudinal displacement of amplitude d, and will not change position laterally; The aircraft in bold then has to move backward a displacement of amplitude d first and then make a lateral position change which is exactly $\sqrt{2}d$.

4.2 Simulations

For comparison purposes, this section presents simulations of traffic under the same initial conditions as described in Chapter 3. The goal of the simulations is also to provide experimental test to the previous theoretical analysis.

We will assume in the first two and the fourth subsections that the aircraft resolve conflicts via lateral and longitudinal position changes. We restrict the backward and forward displacements to be no greater than 5 nm, $i.e.$, $b = f = d = 5$ nm. Simulations and discussion for velocity change maneuvers will be given in the third subsection. For experiments in this subsection, each aircraft has the initial speed of 500 knots, and the speed is restricted to vary without exceeding [475, 525] knots during the conflict resolution.
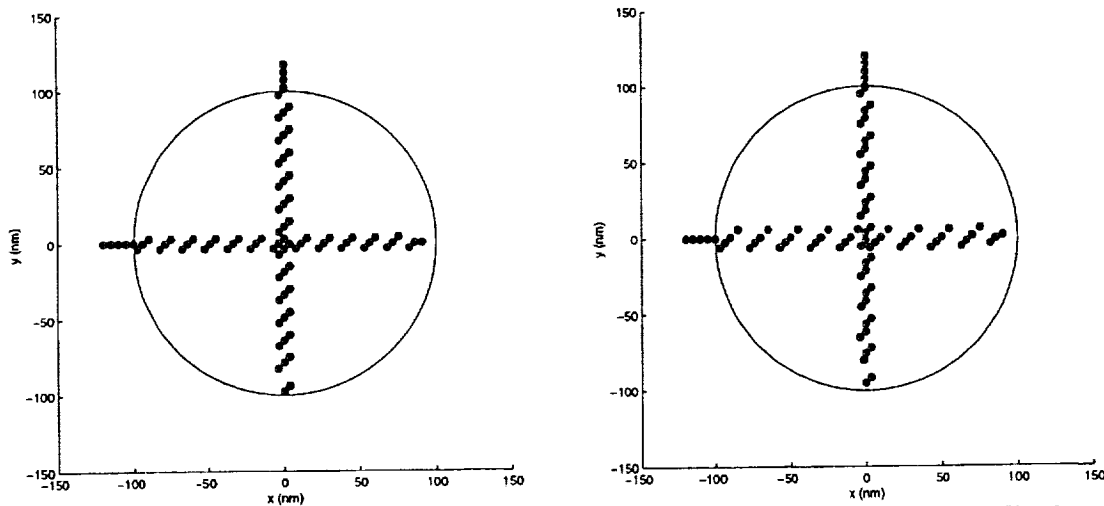
47

Figure 4-4: Test cases for uniform arrival geometry using the offset model. The largest backward and forward displacements are restricted to be 5 nm. The separation distance is 5 nm. Left: In-turn arrival geometry. Right: simultaneous arrival geometry.

4.2.1 Random Arrival Geometry

We first examine the lateral displacement of aircraft in two intersecting streams for random arrival patterns. The aircraft in either stream are initially separated by a distance chosen from a uniform distribution over the interval $[5, 10]$ nm, and a total of 500 aircraft have been simulated. Fig. 4-3 gives a snapshot of the traffic flow taken during the conflict resolution process. Also shown in Fig. 4-3 is a histogram of the lateral deviations experienced by the 500 tested aircraft. The largest lateral displacement found in this simulation is 5.3 nm. The average of the (absolute) lateral displacement over all aircraft is 1.5 nm, and 23.8% of the 500 tested aircraft deviate laterally more than half of the upper bound. Fig. 4-3 also shows that a relatively large number of aircraft have deviated with a lateral displacement of $\sqrt{2}d/2$. This deviation corresponds to an offset maneuver by which the maneuvering aircraft could hide inside the aisle of its "neighbor" and keep contact with this neighbor, while this neighboring aircraft does not deviate sideways.

4.2.2 Uniform Arrival Geometry

We then consider the conflict resolution problem for two aircraft streams with fixed initial separation distance, shown in Fig. 4-4.
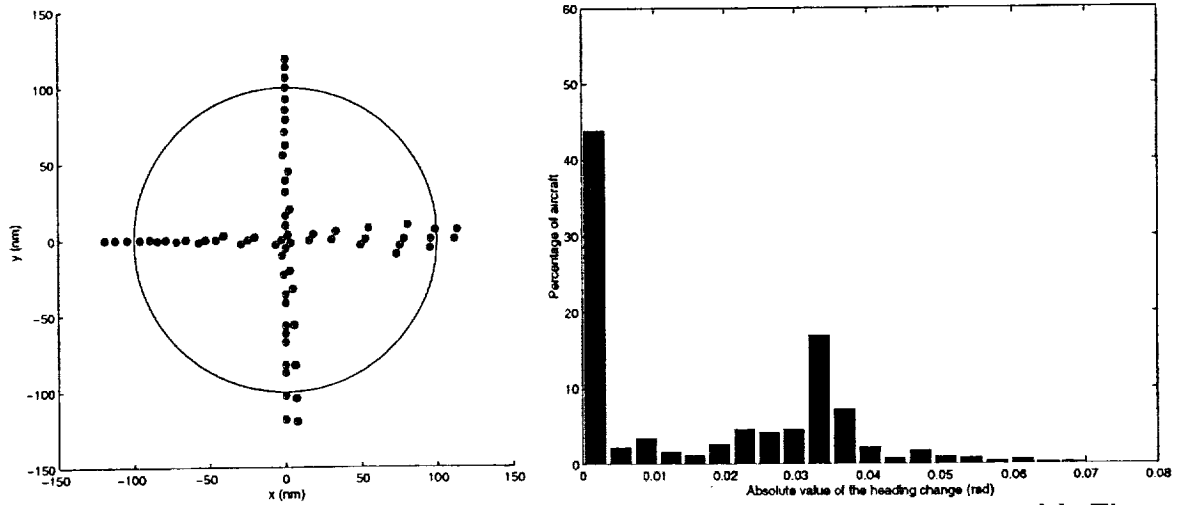
48

Figure 4-5: Test case for random arrival geometry using the velocity change model. The speed of each aircraft is allowed to vary within [475, 525] knots. The separation distance is subject to a uniform distribution on the interval [5, 10] nm, and the number of the tested aircraft is 500. Left: A snapshot taken during the conflict resolution process. Right: Aircraft deviation distribution.

For the case shown on the left of Fig. 4-4, the initial separation distance between every pair of neighboring aircraft is $S = d = 5$ nm, and $d_{s,0} - d_{e,0}$ is chosen to be $S/2$. The example shown on the right of Fig. 4-4 considers the case when $d_{s,0} - d_{e,0}$ decreases to 0.

Fig. 4-4 shows the structure of the traffic flow after conflict resolution. In the example with in-turn arrival geometry (left picture), the largest lateral displacement experienced by the aircraft is 4.2 nm. In the example with simultaneous arrival geometry (right picture), the largest aircraft deviation is 6.8 nm, which is very close to the estimated upper bound (7.1 nm).

From the above two examples we also observe that uniform aircraft arrival flows generate periodic, conflict-free aircraft flow patterns, and the conflict avoidance rule groups the aircraft in "platoons", which are quite similar to those observed in the simulations of the previous chapter but are grouped in a more compact manner.

4.2.3 Stability Results for Velocity Change Model

Simulations in this subsection are designed to compare qualitative aircraft behaviors under the velocity change model with that observed under the offset model. We
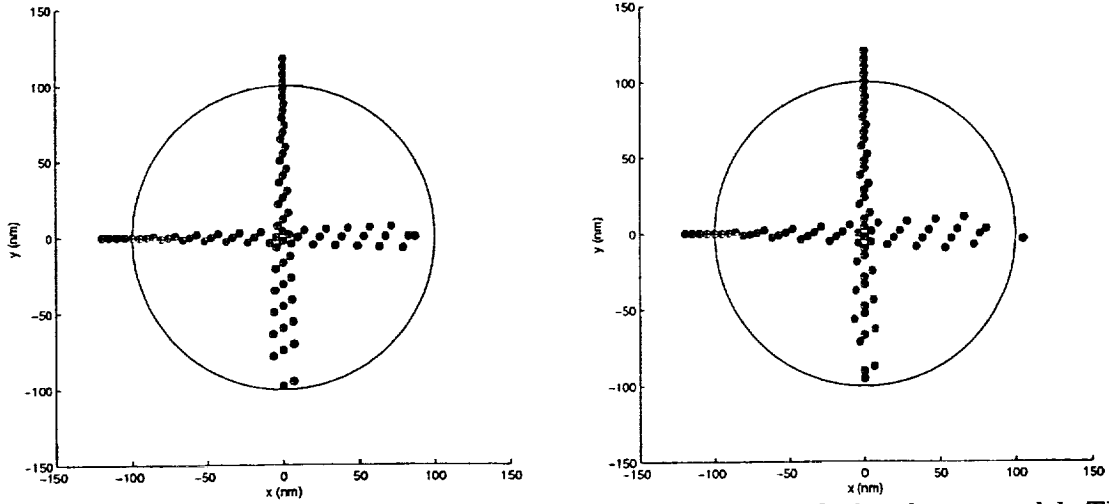
49

Figure 4-6: Test cases for uniform arrival geometry using the velocity change model. The speed of each aircraft is allowed to vary within [475, 525] knots. The separation distance is 5 nm. Left: In-turn arrival geometry. Right: Simultaneous arrival geometry.

assume in this subsection that each aircraft attempts to minimize its heading change, with its speed change being restricted within [475, 525] knots during the conflict resolution.

The first simulation is run under the same conditions as described in the simulation of Fig. 4-3. In Fig. 4-5, the aircraft in each stream are initially separated by a distance chosen from a uniform distribution on the interval [5, 10] nm. Fig. 4-5 (left picture) gives a snapshot taken during the conflict resolution process, while Fig. 4-5 (right picture) shows the distribution of the heading changes for the 500 tested aircraft. There is significant similarity between the two distributions in Fig. 4-3 and Fig. 4-5.

The next two simulations, as shown in Fig. 4-6, consider the same scenarios as described in Fig. 4-4, but use the velocity change model to resolve conflicts. The initial separation distance of aircraft is $S = 5$ nm for both figures. Fig. 4-6 shows the structures of the resulting traffic flows, which are similar to that observed in Fig. 4-4. Note that in the these two simulations we ignored the slight jostling which may possibly occur between two neighboring aircraft.

The examples presented above support the conclusion that the offset model is a good approximation to the velocity change model.
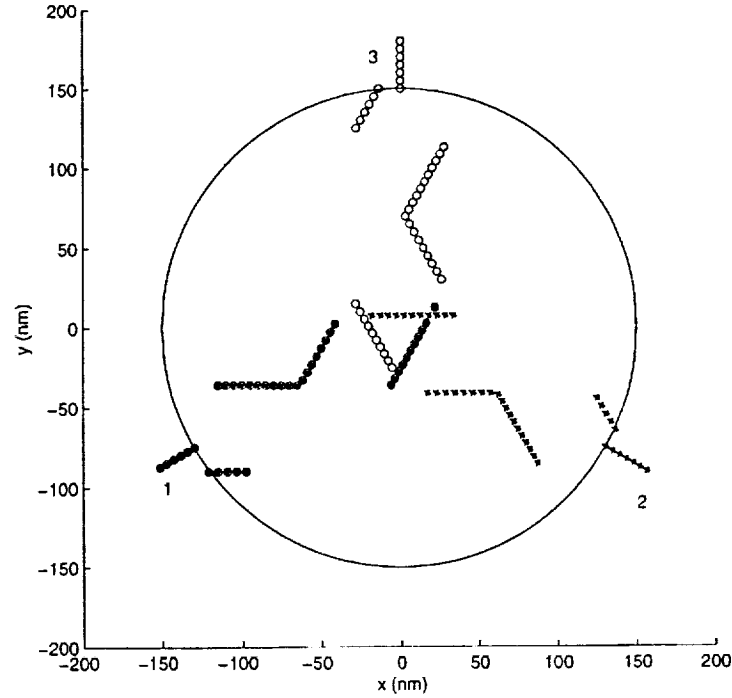
Figure 4-7: Test case for three aircraft flows with uniform and simultaneous arrival geometry using the offset model. The initial separation distance is 5 nm. The largest lateral displacement experienced by the first 105 aircraft is 30.4 nm. (In the plot, we use different symbols to represent the aircraft from different streams.)

4.2.4 Three Aircraft Flow Streams

Considering a problem of three aircraft streams, initially conditioned as same as the problem in Fig. 3-14: The initial separation distance of aircraft is $S = 5$ nm, and the aircraft from each stream enter the conflict area simultaneously. This time the decentralized resolution is performed under the offset model. Compared with the resolution under lateral offset model, Fig. 4-7 shows a new platooning pattern of aircraft, where the linear structure observed in Fig. 3-14 has been cut into "pieces" as presented in Fig.4-7. The largest lateral displacement of the 105 tested aircraft is 30.4 nm.

4.3   General Penalty Functions

4.3.1   An Example

In the previous two sections, we considered the conflict resolution problem for two aircraft flows with both longitudinal and lateral position displacements, based on
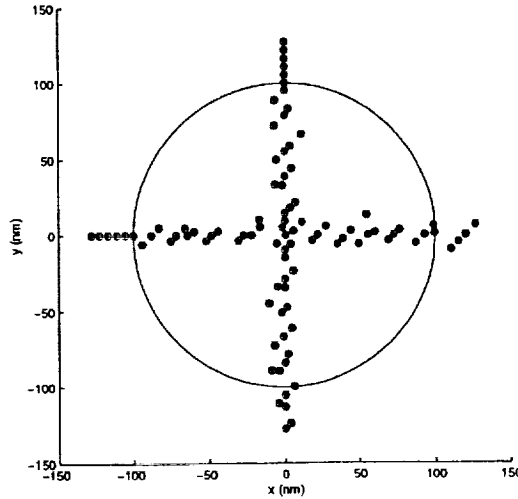
Figure 4-8: An example of conflict resolution for the aircraft using different types of penalty functions. The initial separation distance is subject to a uniform distribution on the interval [5, 6] nm.

the choice of penalty functions which emphasize on minimizing the lateral position change. Under such penalty functions, we have shown that the lateral displacements of any aircraft in the two streams are bounded by $\sqrt{2}d$. This performance bound is tight, and is exactly the same as the bound for the lateral offset model.

Now we ask the following question: Assuming the aircraft may use other types of penalty functions, and each aircraft may use different penalty functions for decision making, will the whole system keep running correctly? The answer to this question will be given in the following subsections.

In this subsection, we present an example showing that the lateral displacements of aircraft could greatly exceed $\sqrt{2}d$ if the aircraft use different penalty functions. Considering two intersecting streams, the aircraft in either stream are initially separated by a random distance subject to a uniform distribution over the interval [5, 6] nm. The aircraft in each stream are randomly chosen from the following two types with equal probabilities: One type of aircraft resolve conflict via lateral position change only, and the other type of aircraft use both lateral and longitudinal changes for conflict resolution as described in Chapter 4.1. A total of 200 aircraft have been simulated. Fig. 4-8 gives a snapshot of the traffic flow taken during the conflict resolution process. The largest lateral displacement found in this simulation is 14.0 nm, approximately twice the value of $\sqrt{2}d$, and 11% of the 200 tested aircraft deviate

52

laterally more than $\sqrt{2}d$.

4.3.2 Penalty Functions and Conflict Resolution

Consider two streams of aircraft as described in Sections 3.1 and 4.1. The eastbound aircraft are denoted as E_i, $i = 1, 2, ...$, and the southbound aircraft are denoted as S_j, $j = 1, 2, ...$ The x and y axes are chosen such that the eastbound aircraft are originally located on the x axis and the southbound aircraft on the y axis, and the two streams of aircraft are flying towards the positive directions of the two axes, respectively. The circular control volume (conflict area) is centered at the origin with radius R. Without loss of generality, we assume that the next aircraft to perform the resolution maneuver is eastbound, and is denoted as E_i.

In the following we focus our attention at the moment when E_i enters the control volume. Denote $(x_{E_k,0}, y_{E_k,0})$ as the original position of aircraft E_k, $k = 1, ..., i$, and (x_{E_k}, y_{E_k}) the expected position after resolution. Denote $\Delta x_{E_k} = x_{E_k} - x_{E_k,0}$ and $\Delta y_{E_k} = y_{E_k} - y_{E_k,0}$. We use $(\Delta x_{E_k}, \Delta y_{E_k})$, the relative position deviation vector to represent the offset maneuver (or resolution) made by aircraft E_k, and use $P_{E_k}(\Delta x_{E_k}, \Delta y_{E_k})$ to represent the penalty function of aircraft E_k. For the southbound aircraft S_l, $l = 1, ..., j$, the subscript of the notations will change to S_l accordingly.

Our proof of stability in this section does not require the penalty functions to be the same for all the aircraft. Given an aircraft A (A could be E_k or S_l), the penalty function of A only needs to satisfy the following conditions: For any Δx_A, $\Delta x'_A$, Δy_A, and $\Delta y'_A$,

- $P_A(\Delta x_A, \Delta y_A) < P_A(\Delta x'_A, \Delta y_A)$ if $|\Delta x_A| < |\Delta x'_A|$;

- $P_A(\Delta x_A, \Delta y_A) < P_A(\Delta x_A, \Delta y'_A)$ if $|\Delta y_A| < |\Delta y'_A|$.

Any norm on the position offset $(\Delta x_A, \Delta y_A)$ satisfies the above two conditions.

As in the previous sections, we would assume that the largest backward and forward displacement of each aircraft is restricted to be no greater than the safety distance d.

53

Then the conflict resolution for aircraft E_i is equivalent to finding a solution to the following optimization problem:

$$\text{minimize } P_{E_i}(\Delta x_{E_i}, \Delta y_{E_i}) \tag{4.2}$$

subject to

$$
\begin{aligned}
d_{E_i,S_l} &\geq d, \quad l = 1, ..., j, \\
d_{E_i,E_k} &\geq d, \quad k = 1, ..., i-1, \\
|\Delta x_{E_i}| &\leq d,
\end{aligned}
\tag{4.3}
$$

where $d_{A,B}$ is the miss distance between aircraft A and B.

4.3.3 Performance Bounds

We now show that, under the proposed decentralized conflict resolution rules and penalty functions for the aircraft flows, an aircraft entering the control volume can always execute a position change maneuver that results in a conflict-free trajectory. A statement of this conclusion with an estimate of system performance bound is presented in Theorem 4.1.

Theorem 4.1: There exists at least one optimal solution to problem (4.2). Let $(\Delta x_{E_i}, \Delta y_{E_i})$ be an optimal solution. Then $|\Delta y_{E_i}|$, the lateral displacement of E_i, is bounded by $\frac{5d}{2} + 2\sqrt{2}d$.

This theorem is proved based on the following three lemmas.

Lemma 4.1: Let $(\Delta x_{E_i}, \Delta y_{E_i})$ be an optimal solution to problem (4.2). If there exists a lateral position change maneuver $(0, \Delta y_{E_i}^o)$ which is conflict-free for aircraft E_i, then $|\Delta y_{E_i}^o|$ is an upper bound for $|\Delta y_{E_i}|$, the lateral displacement of E_i.

Proof: Since $(0, \Delta y_{E_i}^o)$ is a feasible solution and $(\Delta x_{E_i}, \Delta y_{E_i})$ is an optimal solution of
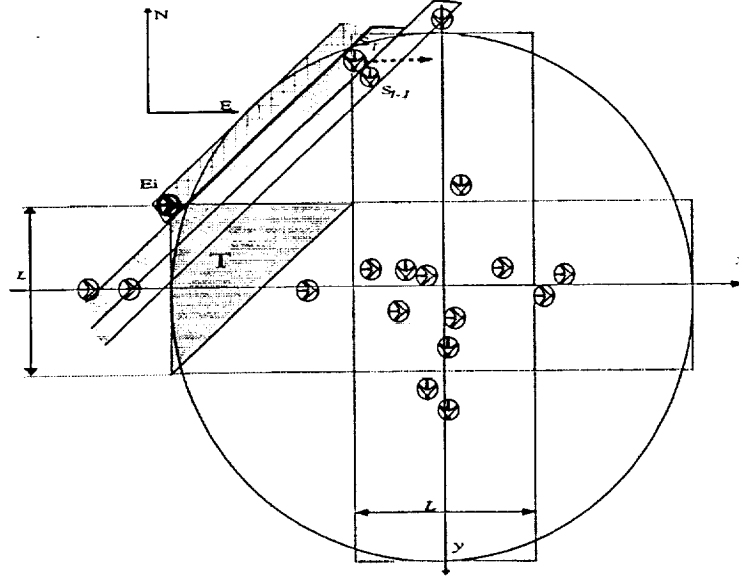
Figure 4-9: Illustration of existence of conflict resolution for Lemma 4.2.

problem (4.2), we have $P_{E_i}(\Delta x_{E_i}, \Delta y_{E_i}) \leq P_{E_i}(0, \Delta y_{E_i}^o)$. According to the property of the penalty function, we have $P_{E_i}(0, \Delta y_{E_i}) \leq P_{E_i}(\Delta x_{E_i}, \Delta y_{E_i}) \leq P_{E_i}(0, \Delta y_{E_i}^o)$, hence $|\Delta y_{E_i}| \leq |\Delta y_{E_i}^o|$. **Q.E.D.**

Lemma 4.2: If $x_{E_i,0} \leq x_{E_{i-1}} - d$ (i.e., when moving laterally only, aircraft E_i has no conflict with the eastbound aircraft ahead of it), then there exists at least one optimal solution to problem (4.2). Further, the lateral displacement of E_i, $|\Delta y_{E_i}|$, is bounded by $2\sqrt{2}d$.

Proof: We begin with the hypothesis that there does not exist such a maneuver with lateral displacement less than or equal to $2\sqrt{2}d$.

In the following, we only consider the lateral position change maneuver of aircraft E_i: $(0, \Delta y_{E_i}^o)$. From the above hypothesis, $|\Delta y_{E_i}^o|$ must be greater than $2\sqrt{2}d$. Otherwise, if $|\Delta y_{E_i}^o| \leq 2\sqrt{2}d$, then by Lemma 4.1 the lateral displacement of E_i is bounded by $|\Delta y_{E_i}^o| \leq 2\sqrt{2}d$, which is contradictory with the hypothesis.

We also know from the hypothesis that the aisles of the eastbound aircraft ahead of E_i should not cover the protected circle of E_i, wherever aircraft E_i is laterally located within the maneuver corridor of total width $L = 4\sqrt{2}d$ centered along the nominal path. That is to say there should not exist any aircraft in the shaded triangular area

55

T in Fig. 4-9. Otherwise, E_i could find a safe location within the maneuver corridor by hiding its protected circle inside the aisle of such aircraft.

At the same time, the maneuvered southbound aircraft have performed conflict resolutions which minimize their penalty functions, and their aisles intersect the protected circle of E_i, wherever E_i is located within the maneuver corridor. Especially at least one aisle of a southbound aircraft, say, S_l, intersects the protected circle of E_i when E_i deviates fully to the left. For this to happen, $x_{S_l} + y_{S_l}$ must be less than $(x_{E_i,0} + 0) + (y_{E_i,0} - L/2) + \sqrt{2}d = -R - 2\sqrt{2}d + \sqrt{2}d$, i.e.,

$$x_{S_l} + y_{S_l} < -R - \sqrt{2}d. \tag{4.4}$$

Next we show by enumeration that (4.4) is contradictory with the optimality assumption we made for the maneuver of S_l.

Case 1: $\Delta y_{S_l} \leq 0$, and S_l is not in contact with S_{l-1}. We know that $y_{S_l} \geq y_{S_l,0} - d \geq -R - d$. So from (4.4), $x_{S_l} < -R - \sqrt{2}d - (-R - d) = -\sqrt{2}d + d < 0$. Since S_l is not in contact with S_{l-1}, we could laterally move S_l a little bit closer to the y axis without "jostling" S_{l-1}, i.e., we could find a $\Delta x'_{S_l}$ which satisfies (1) $\Delta x_{S_l} < \Delta x'_{S_l} < 0$ and (2) with offset maneuver $(\Delta x'_{S_l}, \Delta y_{S_l})$ aircraft S_l is not in contact with S_{l-1}. Hence, with such maneuver, S_l will not be in conflict with any southbound aircraft ahead of it. Also we could see that with the new position change, the aisle of S_l will not overlap any aisles of the eastbound aircraft, i.e., S_l will not be in conflict with the maneuvered eastbound aircraft. Further, $P_{S_l}(\Delta x'_{S_l}, \Delta y_{S_l}) < P_{S_l}(\Delta x_{S_l}, \Delta y_{S_l})$ for $|\Delta x'_{S_l}| < |\Delta x_{S_l}|$. So $(\Delta x'_{S_l}, \Delta y_{S_l})$ is a "better" resolution than $(\Delta x_{S_l}, \Delta y_{S_l})$, which is contradictory with the assumption that $(\Delta x_{S_l}, \Delta y_{S_l})$ is an optimal maneuver.

Case 2: $\Delta y_{S_l} \leq 0$, and S_l is in contact with S_{l-1}. In Case 2, we further consider the following four sub-cases (please refer to Fig. 4-10):

Case 2.1: $x_{S_{l-1}} < 0$ and $x_{S_l} \geq 0$. From (4.4) we can derive $y_{S_l} < -R - \sqrt{2}d$, which is contradictory with $y_{S_l} \geq y_{S_l,0} - d \geq -R - d$.

Case 2.2: $x_{S_{l-1}} < 0$, $x_{S_l} < 0$, and $x_{S_{l-1}} \leq x_{S_l}$. It is easy to see that in this case $(0, \Delta y_{S_l})$ is also a conflict-free resolution for S_l. Since $|\Delta x_{S_l}| > 0$, we have
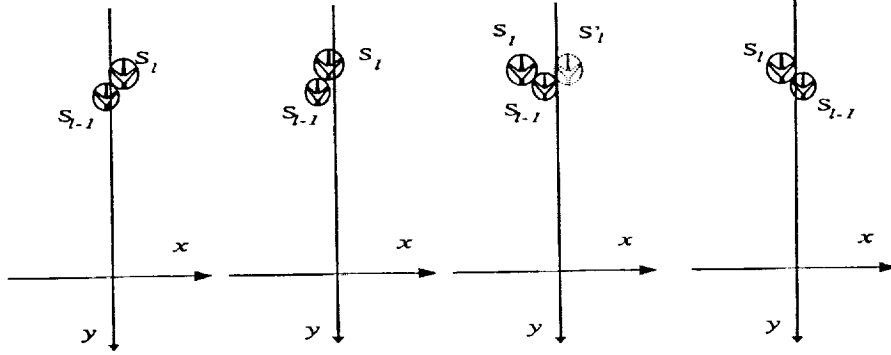
Figure 4-10: Illustrations of some relative positions of S_l and S_{l-1} when $\Delta y_{S_l} \leq 0$ and S_l is in contact with S_{l-1}. From left to right: (1) $x_{S_{l-1}} < 0$ and $x_{S_l} \geq 0$; (2) $x_{S_{l-1}} < 0$, $x_{S_l} < 0$, and $x_{S_{l-1}} \leq x_{S_l}$; (3) $x_{S_{l-1}} < 0$, $x_{S_l} < 0$, and $x_{S_{l-1}} > x_{S_l}$; (4) $x_{S_{l-1}} \geq 0$.

$P_{S_l}(0, \Delta y_{S_l}) < P_{S_l}(\Delta x_{S_l}, \Delta y_{S_l})$, which is contradictory with the optimality assumption for $(\Delta x_{S_l}, \Delta y_{S_l})$.

Case 2.3: $x_{S_{l-1}} < 0$, $x_{S_l} < 0$, and $x_{S_{l-1}} > x_{S_l}$. Let $\Delta x'_{S_l} = 2x_{S_{l-1}} - x_{S_l}$. Obviously, $|\Delta x'_{S_l}| < |\Delta x_{S_l}|$. And it can be tested that $(\Delta x'_{S_l}, \Delta y_{S_l})$ is a conflict-free resolution for S_l. Therefore, $(\Delta x'_{S_l}, \Delta y_{S_l})$ is a "better" conflict resolution than $(\Delta x_{S_l}, \Delta y_{S_l})$. Again this causes contradiction with the optimality assumption.

Case 2.4: $x_{S_{l-1}} \geq 0$. Since S_l is in contact with S_{l-1}, we can derive

$$x_{S_l} + y_{S_l} \geq x_{S_{l-1}} + y_{S_{l-1}} - \sqrt{2}d. \tag{4.5}$$

According to both (4.4) and (4.5), we have $x_{S_{l-1}} + y_{S_{l-1}} \leq x_{S_l} + y_{S_l} + \sqrt{2}d < -R$. At the same time, since $y_{S_{l-1}} \geq -R$ and $x_{S_{l-1}} \geq 0$, we have $x_{S_{l-1}} + y_{S_{l-1}} \geq -R$. These two inequalities are contradictory with each other.

Case 3: $\Delta y_{S_l} > 0$. In this case, S_l must be in contact with S_{l-1}, and further $y_{S_l} > y_{S_{l-1}}$. Otherwise, we could longitudinally move S_l backwards a little bit without "jostling" S_{l-1}, i.e., we can construct a new resolution maneuver $(\Delta x_{S_l}, \Delta y'_{S_l})$ with $0 < \Delta y'_{S_l} < \Delta y_{S_l}$ for S_l such that (1) S_l is not in contact with any southbound aircraft S_k, $k < l$; (2) S_l is not in conflict with any eastbound aircraft E_j, $j < i$. Therefore $(\Delta x_{S_l}, \Delta y'_{S_l})$ is a resolution with smaller penalty function value than that
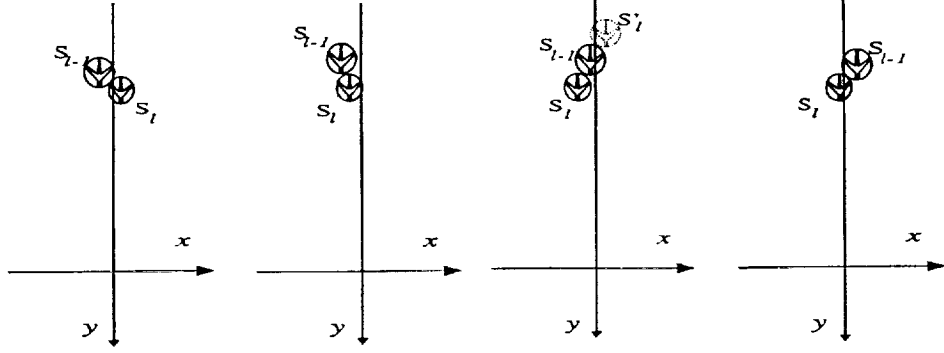
Figure 4-11: Illustrations of some relative positions of S_l and S_{l-1} when $\Delta y_{S_l} > 0$. From left to right: (1) $x_{S_{l-1}} < 0$ and $x_{S_l} \geq 0$; (2) $x_{S_{l-1}} < 0$, $x_{S_l} < 0$, and $x_{S_{l-1}} \leq x_{S_l}$; (3) $x_{S_{l-1}} < 0$, $x_{S_l} < 0$, and $x_{S_{l-1}} > x_{S_l}$; (4) $x_{S_{l-1}} \geq 0$.

of $(\Delta x_{S_l}, \Delta y_{S_l})$, which is contradictory with the optimality assumption we made for the maneuver of S_l.

In Case 3, we further consider the following four sub-cases (please refer to Fig. 4-11):

Case 3.1: $x_{S_{l-1}} < 0$ and $x_{S_l} \geq 0$. From (4.4) we can derive $y_{S_l} < -R - \sqrt{2}d$, which is contradictory with $y_{S_l} \geq y_{S_{l,0}} \geq -R$.

Case 3.2: $x_{S_{l-1}} < 0$, $x_{S_l} < 0$, and $|x_{S_l}| \leq |x_{S_{l-1}}|$. Because of the relative location of S_l with respect to S_{l-1}, it can be tested that the following two situations can not occur simultaneously: (1) S_{l-1} is in contact with some S_k ($k < l - 1$) and $x_{S_k} > x_{S_{l-1}}$; (2) S_l is in contact with some S_k ($k < l - 1$) and $x_{S_k} > x_{S_l}$. If situation (1) does not happen, then we can laterally move S_{l-1} a little bit closer to the y axis without "jostling" any other southbound aircraft ahead of it, i.e., we can construct a new resolution maneuver $(\Delta x'_{S_{l-1}}, \Delta y_{S_{l-1}})$ with $\Delta x_{S_{l-1}} < \Delta x'_{S_{l-1}} < 0$ for S_{l-1} such that S_{l-1} is not in contact with any southbound aircraft S_k ($k < l - 1$) and S_{l-1} is not in conflict with any eastbound aircraft E_j ($j < i$). Therefore $(\Delta x'_{S_{l-1}}, \Delta y_{S_{l-1}})$ is a resolution with smaller penalty function value than that of $(\Delta x_{S_{l-1}}, \Delta y_{S_{l-1}})$, which is contradictory with the optimality assumption we made for the maneuver of S_{l-1}. Similarly, if situation (2) does not happen, then we can construct a "better" resolution for S_l by laterally moving S_l a little bit closer to the y axis without "jostling" any

southbound aircraft, therefore inducing contradiction with the optimality assumption.

Case 3.3: $x_{S_{l-1}} < 0$, $x_{S_l} < 0$, and $|x_{S_l}| > |x_{S_{l-1}}|$. Let $x'_{S_l} = 2x_{S_{l-1}} - x_{S_l}$ and $y'_{S_l} = 2y_{S_{l-1}} - y_{S_l}$. Obviously, $|\Delta x'_{S_l}| < |\Delta x_{S_l}|$ and $|\Delta y'_{S_l}| \leq |\Delta y_{S_l}|$ (because $\Delta y_{S_l} > 0$ and $y_{S_{l-1}} \geq y_{S_{l-1},0} - d \geq y_{S_l,0}$). And it can be tested that $(\Delta x'_{S_l}, \Delta y'_{S_l})$ is a conflict-free resolution for S_l. Therefore, $(\Delta x'_{S_l}, \Delta y'_{S_l})$ is a "better" conflict resolution than $(\Delta x_{S_l}, \Delta y_{S_l})$. Again this causes contradiction with the optimality assumption.

Case 3.4: $x_{S_{l-1}} \geq 0$. Since S_l is in contact with S_{l-1}, we can derive

$$x_{S_l} + y_{S_l} \geq x_{S_{l-1}} + y_{S_{l-1}} - \sqrt{2}d. \tag{4.6}$$

According to both (4.4) and (4.6), we have $x_{S_{l-1}} + y_{S_{l-1}} \leq x_{S_l} + y_{S_l} + \sqrt{2}d < -R$. At the same time, since $y_{S_{l-1}} \geq -R$ and $x_{S_{l-1}} \geq 0$, we have $x_{S_{l-1}} + y_{S_{l-1}} \geq -R$. These two inequalities are contradictory with each other.

From the above discussion, we have induced contradiction based on the hypothesis we made at the beginning of this proof. So the hypothesis can not hold. Therefore, we prove that $2\sqrt{2}d$ is an upper bound for the lateral displacement of E_i. Q.E.D.

We have considered the aircraft flow stability for the case of $x_{E_i,0} \leq x_{E_{i-1}} - d$. For the case of $x_{E_i,0} > x_{E_{i-1}} - d$, the argument in the above proof is no longer valid, because aircraft E_i, when moving laterally only, may not be able to hide inside the aisles of some eastbound aircraft due to the possible "push" from aircraft E_{i-1}. Before proceeding with our further discussion, we define a region $\{(x, y) | x_{E_{i-1}} + y_{E_{i-1}} - d_1 < x + y < x_{E_{i-1}} + y_{E_{i-1}} + d_2\}$ called the *forbidden region*, which is an aisle that totally covers the aisle of E_{i-1} and does not overlap the aisle of any southbound aircraft. The forbidden region has the property that aircraft E_i could not safely hide its protected circle inside the forbidden region because of the push from aircraft E_{i-1}. It can be tested that d_1 and d_2 should satisfy:

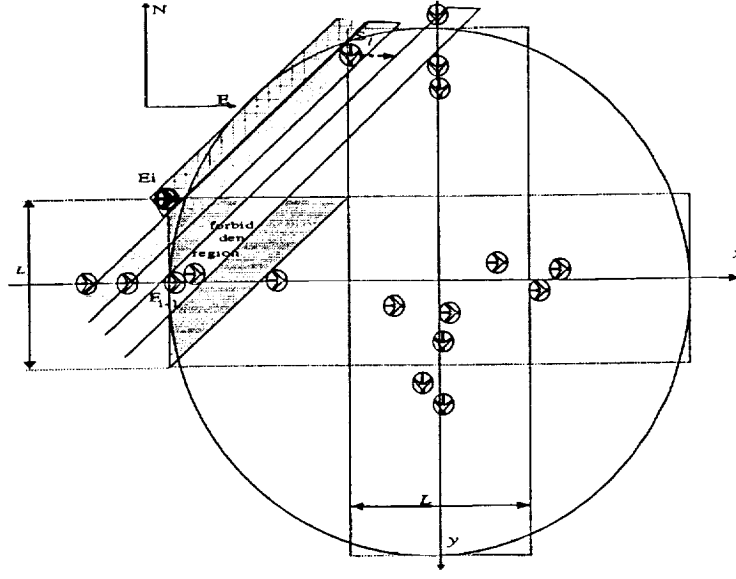$$d_1 + d_2 \leq 2d + \sqrt{2}d. \tag{4.7}$$

Figure 4-12: Illustration of existence of conflict resolution for Lemma 4.3..

Lemma 4.3: If $x_{E_i,0} > x_{E_i-1} - d$, then there exists at least one optimal solution to problem (4.2). Further, the lateral displacement of E_i, $|\Delta y_{E_i}|$, is bounded by $\frac{5d}{2} + 2\sqrt{2}d$.

Proof: Consider the maneuver corridor centered at the x axis with width $L = 5d + 4\sqrt{2}d$. Again we proceed with the proof by contradiction: First assume that there does not exist such a maneuver with lateral displacement less than or equal to $L/2$.

In this proof we only consider the lateral offset maneuver of aircraft E_i: $(0, \Delta y_{E_i}^o)$. The above assumption implies that $|\Delta y_{E_i}^o| > L/2$. Otherwise, if $|\Delta y_{E_i}^o| \leq L/2$, then by Lemma 4.1 the lateral displacement of E_i is bounded by $L/2$, which is contradictory with the assumption.

Please refer to Fig. 4-12. There should not exist any aircraft in the shaded area - a triangular area excluding the forbidden region in Fig. 4-12. Otherwise, E_i could find a location within the maneuver corridor by hiding inside the aisle of such aircraft. At the same time, any maneuvered southbound aircraft must have performed conflict resolutions which minimize their penalty functions. Therefore, there exists a southbound aircraft, denoted as S_l, satisfying

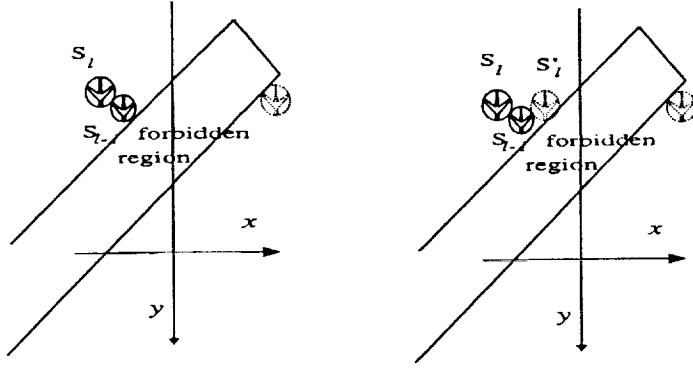$$x_{S_l} + y_{S_l} < -R - L/2 + \sqrt{2}d,$$

60

Figure 4-13: Illustrations of some relative positions of S_l and S_{l-1} when $\Delta y_{S_l} \leq 0$ and S_l is in contact with S_{l-1}. Left: S_{l-1} is in contact with the forbidden region. Right: S_{l-1} is not in contact with the forbidden region, and $x_{S_{l-1}} < 0$.

i.e.,

$$x_{S_l} + y_{S_l} < -R - \frac{5d + 2\sqrt{2}d}{2}. \tag{4.8}$$

Next we show by enumeration that (4.8) is contradictory with the optimality assumption we made for the maneuver of S_l.

Case 1: $\Delta y_{S_l} \leq 0$, and S_l is in contact with S_{l-1}. Since $\Delta y_{S_l} \leq 0$, there must be $y_{S_l} \leq y_{S_{l-1}}$. In Case 1, we further consider the following three sub-cases.

Case 1.1: S_{l-1} is in contact with the forbidden region (please refer to Fig. 4-13 (the left picture)). It is easy to see that in this case

$$x_{S_{l-1}} + y_{S_{l-1}} = x_{E_{i-1}} + y_{E_{i-1}} - d_1 - \sqrt{2}d/2.$$

Since S_l is in contact with S_{l-1}, we have

$$x_{S_l} + y_{S_l} \geq x_{S_{l-1}} + y_{S_{l-1}} - \sqrt{2}d.$$

Hence

$$x_{S_l} + y_{S_l} \geq x_{E_{i-1}} + y_{E_{i-1}} - d_1 - 3\sqrt{2}d/2,$$

61

or

$$-x_{S_l} - y_{S_l} \leq -x_{E_{i-1}} - y_{E_{i-1}} + d_1 + 3\sqrt{2}d/2. \tag{4.9}$$

As $(\Delta x_{S_l}, \Delta y_{S_l})$ is an optimal maneuver for S_l, its penalty function value must be no greater than any feasible (conflict-free) maneuver of S_l on the other side of the forbidden region. Especially, considering for S_l the "best" conflict-free lateral offset maneuver $(\Delta x_{S_l}^o, 0)$ on the other side of the forbidden region, we have $|\Delta x_{S_l}^o| \geq |\Delta x_{S_l}|$. Further, $\Delta x_{S_l}^o$ must be greater than 0; Otherwise, from the relative positions of $(x_{S_l}^o, y_{S_{l,0}})$, (x_{S_l}, y_{S_l}), and the y axis, there should be $|\Delta x_{S_l}^o| < |\Delta x_{S_l}|$, which is contradictory to $|\Delta x_{S_l}^o| \geq |\Delta x_{S_l}|$. Therefore, at location $(x_{S_l}^o, y_{S_{l,0}})$ S_l must be in contact with the forbidden region, because $\Delta x_{S_l}^o > 0$ and S_l (at location $(x_{S_l}^o, y_{S_{l,0}})$) can not be jostled by any other southbound aircraft S_k, $k < l$. Then we have

$$x_{S_l}^o + y_{S_{l,0}} = x_{E_{i-1}} + y_{E_{i-1}} + d_2 + \sqrt{2}d/2,$$

i.e.,

$$x_{S_l}^o = -y_{S_{l,0}} + x_{E_{i-1}} + y_{E_{i-1}} + d_2 + \sqrt{2}d/2. \tag{4.10}$$

Taking into account that $y_{S_l} \geq y_{S_{l,0}} - d$, we induce from (4.10) the following inequality

$$x_{S_l}^o - y_{S_l} \leq -2y_{S_{l,0}} + x_{E_{i-1}} + y_{E_{i-1}} + d_2 + d + \sqrt{2}d/2.$$

Since $\Delta x_{S_l}^o > 0$, $|\Delta x_{S_l}^o| \geq |\Delta x_{S_l}|$ implies $\Delta x_{S_l}^o \geq -\Delta x_{S_l}$ or $x_{S_l}^o \geq -x_{S_l}$. Then we have

$$-x_{S_l} - y_{S_l} \leq -2y_{S_{l,0}} + x_{E_{i-1}} + y_{E_{i-1}} + d_2 + d + \sqrt{2}d/2. \tag{4.11}$$

Adding (4.9) and (4.11) together, we have

$$-2x_{S_l} - 2y_{S_l} \leq -2y_{S_{l,0}} + d_1 + d_2 + d + 2\sqrt{2}d.$$

Since $y_{S_{l,0}} \geq -R$, and according to (4.7), we obtain

$$x_{S_l} + y_{S_l} \geq -R - \frac{3d + 3\sqrt{2}d}{2}. \qquad (4.12)$$

It is easy to see that (4.12) is contradictory with (4.8).

Case 1.2: S_{l-1} is not in contact with the forbidden region, and $x_{S_{l-1}} \geq 0$. Since S_l and S_{l-1} are in contact with each other, $x_{S_{l-1}} \geq 0$ implies $x_{S_l} \geq -d$. As $y_{S_l} \geq -R - d$, and according to (4.8), we have $-d - R - d \leq x_{S_l} + y_{S_l} < -R - \frac{5d + 2\sqrt{2}d}{2}$, inducing contradiction.

Case 1.3: S_{l-1} is not in contact with the forbidden region, and $x_{S_{l-1}} < 0$ (please refer to Fig. 4-13 (the right picture)). Let us consider the offset maneuver $(2\Delta x_{S_{l-1}} - \Delta x_{S_l}, \Delta y_{S_l})$ for S_l. We claim that the protected circle of S_l after this maneuver must overlap the forbidden region. Otherwise, such maneuver is conflict-free. Further, it is easy to test that this maneuver has smaller penalty function value than that of $(\Delta x_{S_l}, \Delta y_{S_l})$. Therefore, $(2\Delta x_{S_{l-1}} - \Delta x_{S_l}, \Delta y_{S_l})$ is a "better" resolution than $(\Delta x_{S_l}, \Delta y_{S_l})$, which is contradictory with the optimality assumption.

Since the protected circle of S_l after maneuver $(2\Delta x_{S_{l-1}} - \Delta x_{S_l}, \Delta y_{S_l})$ overlaps the forbidden region, we have

$$(2x_{S_{l-1}} - x_{S_l}) + y_{S_l} \geq x_{E_{i-1}} + y_{E_{i-1}} - d_1 - \sqrt{2}d/2.$$

For $x_{S_{l-1}} - x_{S_l} \leq d$, we can derive the following inequality from the above one

$$-x_{S_l} - y_{S_l} \leq -x_{E_{i-1}} - y_{E_{i-1}} + d_1 + 2d + \sqrt{2}d/2. \qquad (4.13)$$

Next we follow the discussion in Case 1.1, and could get (4.11). Add (4.13) and (4.11) together, then we have

$$-2x_{S_l} - 2y_{S_l} \leq -2y_{S_{l,0}} + d_1 + d_2 + 3d + \sqrt{2}d.$$
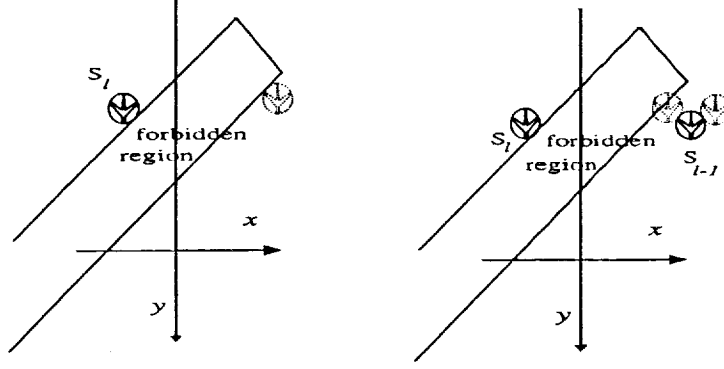
63

Figure 4-14: Illustrations of some relative positions of S_l and S_{l-1} when $\Delta y_{S_l} \leq 0$ and S_l is not in contact with S_{l-1}. Left: At location $(x^o_{S_l}, y_{S_{l,0}})$ (aircraft plotted in dotted lines), S_l is in contact with the forbidden region. Right: At location $(x^o_{S_l}, y_{S_{l,0}})$ (aircraft plotted in dotted lines), S_l is in contact with S_{l-1} and $x_{S_{l-1}} > 0$.

Since $y_{S_{l,0}} \geq -R$, and according to (4.7), we obtain

$$x_{S_l} + y_{S_l} \geq -R - \frac{5d + 2\sqrt{2}d}{2}. \tag{4.14}$$

Obviously, (4.14) is contradictory with (4.8).

Case 2: $\Delta y_{S_l} \leq 0$, and S_l is not in contact with S_{l-1}. It is easy to see that if $\Delta x_{S_l} \geq 0$, it must be true that $|\Delta y^o_{E_i}| < L/2$, which is contradictory with the hypothesis we made previously. So we only need to consider the case of $\Delta x_{S_l} < 0$. Since S_l is not jostled by any southbound aircraft S_k ($k < l$), the aisle of S_l must be in contact with the forbidden region:

$$x_{S_l} + y_{S_l} = x_{E_{i-1}} + y_{E_{i-1}} - d_1 - \sqrt{2}d/2,$$

or

$$-x_{S_l} - y_{S_l} = -x_{E_{i-1}} - y_{E_{i-1}} + d_1 + \sqrt{2}d/2. \tag{4.15}$$

Now we consider for S_l the "best" conflict-free lateral offset maneuver $(\Delta x^o_{S_l}, 0)$ on the other side of the forbidden region, we have $|\Delta x^o_{S_l}| \geq |\Delta x_{S_l}|$. Further $\Delta x^o_{S_l}$ must be greater than 0 (for the reason, please refer to the arguments in Case 1.1).

Therefore, at location $(x^o_{S_l}, y_{S_{l,0}})$, there are only two possibilities for aircraft S_l: Either S_l is in contact with the forbidden region or not (if not, then S_l must be jostled by S_{l-1}). We discuss these two possibilities in the following three sub-cases.

Case 2.1: At location $(x^o_{S_l}, y_{S_{l,0}})$, S_l is in contact with the forbidden region (please refer to Fig. 4-14 (the left picture)). Similar to the discussion in Case 1.1, we have

$$-x_{S_l} - y_{S_l} \leq -2y_{S_{l,0}} + x_{E_{l-1}} + y_{E_{l-1}} + d_2 + d + \sqrt{2}d/2. \qquad (4.16)$$

Add (4.15) and (4.16) together, then we have

$$-2x_{S_l} - 2y_{S_l} \leq -2y_{S_{l,0}} + d_1 + d_2 + d + \sqrt{2}d.$$

Since $y_{S_{l,0}} \geq -R$, and according to (4.7), we obtain

$$x_{S_l} + y_{S_l} \geq -R - \frac{3d + 2\sqrt{2}d}{2}. \qquad (4.17)$$

It is easy to see that (4.17) is contradictory with (4.8).

Case 2.2: At location $(x^o_{S_l}, y_{S_{l,0}})$, S_l is in contact with S_{l-1}, and $x_{S_{l-1}} \leq 0$. Since S_l and S_{l-1} are in contact with each other, $x_{S_{l-1}} \leq 0$ implies $x^o_{S_l} \leq d$. Hence $x_{S_l} \geq -x^o_{S_l} \geq -d$ because of the optimality assumption of maneuver $(\Delta x_{S_l}, \Delta y_{S_l})$. As $y_{S_l} \geq -R - d$, and according to (4.8), we have $-d - R - d \leq x_{S_l} + y_{S_l} < -R - \frac{5d + 2\sqrt{2}d}{2}$, inducing contradiction.

Case 2.3: At location $(x^o_{S_l}, y_{S_{l,0}})$, S_l is in contact with S_{l-1}, and $x_{S_{l-1}} > 0$ (please refer to Fig. 4-14 (the right picture)). Let us consider the offset maneuver $(2\Delta x_{S_{l-1}} - \Delta x^o_{S_l}, 0)$ for S_l. We claim that the protected circle of S_l after this maneuver must overlap the forbidden region. Otherwise, such maneuver is conflict-free. Further, it is easy to test that this maneuver has smaller penalty function value than that of $(\Delta x^o_{S_l}, 0)$. Therefore, $(2\Delta x_{S_{l-1}} - \Delta x^o_{S_l}, 0)$ is a "better" resolution than $(\Delta x^o_{S_l}, 0)$, which is contradictory with the assumption we made for $(\Delta x^o_{S_l}, 0)$.

Since the protected circle of S_l after maneuver $(2\Delta x_{S_{l-1}} - \Delta x^o_{S_l}, 0)$ overlaps the

65

forbidden region, we have

$$(2x_{S_{l-1}} - x^o_{S_l}) + y_{S_{l,0}} \leq x_{E_{i-1}} + y_{E_{i-1}} + d_2 + \sqrt{2}d/2.$$

Since $x_{S_{l-1}} - x^o_{S_l} \geq -d$, we can derive the following inequality from the above one

$$x^o_{S_l} + y_{S_{l,0}} \leq x_{E_{i-1}} + y_{E_{i-1}} + d_2 + 2d + \sqrt{2}d/2.$$

Note that $x^o_{S_l} \geq -x_{S_l}$ and $y_{S_{l,0}} \leq y_{S_l} + d$. So we have

$$-x_{S_l} - y_{S_l} \leq -2y_{S_{l,0}} + x_{E_{i-1}} + y_{E_{i-1}} + d_2 + 3d + \sqrt{2}d/2. \qquad (4.18)$$

Add (4.15) and (4.18) together, then we get

$$-2x_{S_l} - 2y_{S_l} \leq -2y_{S_{l,0}} + d_1 + d_2 + 3d + \sqrt{2}d.$$

Since $y_{S_{l,0}} \geq -R$, according to (4.7), we obtain

$$x_{S_l} + y_{S_l} \geq -R + \frac{5d + 2\sqrt{2}d}{2}. \qquad (4.19)$$

Obviously, (4.19) is contradictory with (4.8).

Case 3: $\Delta y_{S_l} > 0$. In this case, S_l must be in contact with S_{l-1}, and further $y_{S_l} > y_{S_{l-1}}$. Otherwise, we could longitudinally move S_l backwards a little bit without "jostling" S_{l-1}, i.e., we can easily construct a new resolution maneuver $(\Delta x_{S_l}, \Delta y'_{S_l})$ with $0 < \Delta y'_{S_l} < \Delta y_{S_l}$ for S_l such that (1) S_l is not in contact with any southbound aircraft S_k, $k < l$; (2) S_l is not in conflict with any eastbound aircraft E_j, $j < i$. Therefore $(\Delta x_{S_l}, \Delta y'_{S_l})$ is a resolution with smaller penalty function value than that of $(\Delta x_{S_l}, \Delta y_{S_l})$, which is contradictory with the optimality assumption we made for the maneuver of S_l.

In Case 3, we further consider the following three subcases.

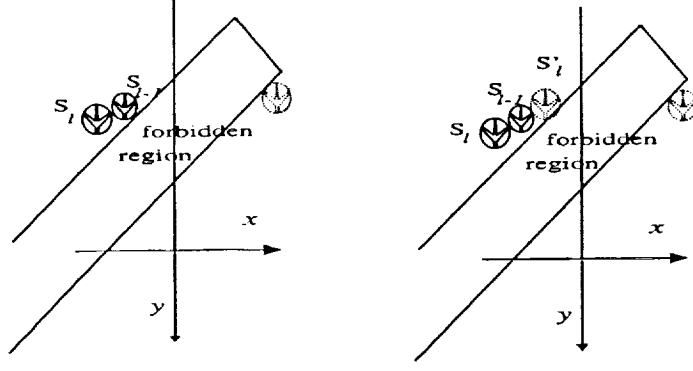Case 3.1: S_{l-1} is in contact with the forbidden region (please refer to Fig. 4-15

66

Figure 4-15: Illustrations of some relative positions of S_l and S_{l-1} when $\Delta y_{S_l} > 0$. Left: S_{l-1} is in contact with the forbidden region. Right: S_{l-1} is not in contact with the forbidden region, and $x_{S_{l-1}} < 0$.

(the left picture)). Obviously,

$$x_{S_{l-1}} + y_{S_{l-1}} = x_{E_{i-1}} + y_{E_{i-1}} - d_1 - \sqrt{2}d/2.$$

Since S_l is in contact with S_{l-1}, we have

$$x_{S_l} + y_{S_l} \geq x_{S_{l-1}} + y_{S_{l-1}} - \sqrt{2}d.$$

Hence

$$x_{S_l} + y_{S_l} \geq x_{E_{i-1}} + y_{E_{i-1}} - d_1 - 3\sqrt{2}d/2,$$

or

$$-x_{S_l} - y_{S_l} \leq -x_{E_{i-1}} - y_{E_{i-1}} + d_1 + 3\sqrt{2}d/2. \qquad (4.20)$$

Following the discussion in Case 1.1, we can also obtain

$$-x_{S_l} - y_{S_l} \leq -2y_{S_{l,0}} + x_{E_{i-1}} + y_{E_{i-1}} + d_2 + d + \sqrt{2}d/2. \qquad (4.21)$$

Adding (4.20) and (4.21) together, we have

$$-2x_{S_l} - 2y_{S_l} \leq -2y_{S_{l,0}} + d_1 + d_2 + d + 2\sqrt{2}d.$$

67

Since $y_{S_l,0} \geq -R$, and according to (4.7), we obtain

$$x_{S_l} + y_{S_l} \geq -R - \frac{3d + 3\sqrt{2}d}{2}. \qquad (4.22)$$

It is easy to see that (4.22) is contradictory with (4.8).

Case 3.2: S_{l-1} is not in contact with the forbidden region, and $x_{S_{l-1}} \geq 0$. Since S_l and S_{l-1} are in contact with each other, $x_{S_{l-1}} \geq 0$ implies $x_{S_l} \geq -d$. As $y_{S_l} \geq -R - d$, and according to (4.8), we have $-d - R - d \leq x_{S_l} + y_{S_l} < -R - \frac{5d + 2\sqrt{2}d}{2}$, inducing contradiction.

Case 3.3: S_{l-1} is not in contact with the forbidden region, and $x_{S_{l-1}} < 0$ (please refer to Fig. 4-15 (the right picture)). In Case 3.3, we only consider the situation when $x_{S_l} < x_{S_{l-1}}$. (When $x_{S_l} \geq x_{S_{l-1}}$, the aisle of aircraft S_{l-1} must intersect the protected circle of E_i when E_i deviates fully to the left. In such case, we would rather choose S_{l-1} as the aircraft under consideration instead of S_l at the beginning of the proof. Since $y_{S_l} > y_{S_{l-1}}$, there should be $\Delta y_{S_{l-1}} < 0$. Then we can induce contradiction by using the arguments in Case 1 and Case 2 upon aircraft S_{l-1}.)

Now let $x'_{S_l} = 2x_{S_{l-1}} - x_{S_l}$ and $y'_{S_l} = 2y_{S_{l-1}} - y_{S_l}$. Obviously, $|\Delta x'_{S_l}| < |\Delta x_{S_l}|$ and $|\Delta y'_{S_l}| \leq |\Delta y_{S_l}|$ (because $\Delta y_{S_l} > 0$ and $y_{S_{l-1}} \geq y_{S_{l-1},0} - d \geq y_{S_l,0}$). So maneuver $(\Delta x'_{S_l}, \Delta y'_{S_l})$ has smaller penalty function value than that of $(\Delta x_{S_l}, \Delta y_{S_l})$. Therefore the protected circle of S_l after maneuver $(\Delta x'_{S_l}, \Delta y'_{S_l})$ must overlap the forbidden region. Otherwise, such maneuver is conflict-free, and as we have shown that it has smaller penalty function value than that of $(\Delta x_{S_l}, \Delta y_{S_l})$, $(\Delta x'_{S_l}, \Delta y'_{S_l})$ is a "better" resolution than $(\Delta x_{S_l}, \Delta y_{S_l})$, which is contradictory with the optimality assumption.

Since the protected circle of S_l after maneuver $(\Delta x'_{S_l}, \Delta y'_{S_l})$ overlaps the forbidden region, we have

$$x'_{S_l} + y'_{S_l} \geq x_{E_{i-1}} + y_{E_{i-1}} - d_1 - \sqrt{2}d/2.$$

For $x_{S_{l-1}} - x_{S_l} \leq d$ and $y_{S_l} \geq y'_{S_l}$, we can derive the following inequality from the above one

$$-x_{S_l} - y_{S_l} \leq -x_{E_{i-1}} - y_{E_{i-1}} + d_1 + 2d + \sqrt{2}d/2. \qquad (4.23)$$

Next we follow the argument in Case 1.1, and can get the same inequality as (4.11). Adding (4.23) and (4.11) together, we have

$$-2x_{S_l} - 2y_{S_l} \leq -2y_{S_{l,0}} + d_1 + d_2 + 3d + \sqrt{2}d.$$

Since $y_{S_{l,0}} \geq -R$, and according to (4.7), we obtain

$$x_{S_l} + y_{S_l} \geq -R - \frac{5d + 2\sqrt{2}d}{2}. \tag{4.24}$$

Obviously, (4.24) is contradictory with (4.8).

From the above discussion, we have induced contradiction based on the hypothesis we made at the beginning of this proof. **Q.E.D.**

It is easy to see that Theorem 4.1 is a direct consequence of Lemma 4.2 and Lemma 4.3.

Chapter 5

Comparison with Centralized

Resolution Strategies

In this chapter, we compare the solutions provided by decentralized conflict resolution strategies with centralized solution strategies that may be obtained for a finite set of aircraft. The goal of this study is to evaluate the degree of "inefficiency" of the decentralized conflict resolution scheme discussed in the earlier chapters.

Our computational approaches (including those presented in this chapter and in [14]) follow the spirit of previous authors: In [29], Niedringhaus proposed linear programming as a convenient modeling framework to formulate and solve efficiently conflicts arising among several aircraft. In [11], Durand, Alliot and Chansou considered the same problem and proposed to use genetic algorithms and linear programming to determine optimal maneuvers to solve conflicts arising among multiple aircraft. While both approaches emphasize (but are not limited to) planar conflict problems, the latter approach differs from the former in that it also optimizes the conflict resolution maneuver over possible *crossing patterns*, whereas the former approach requires *a priori* knowledge of the crossing pattern among aircraft.
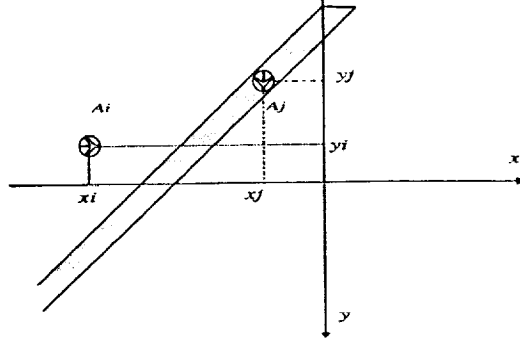
Figure 5-1: Conflict avoidance constraints for offset model.

5.1 Centralized Resolution for Offset Model

5.1.1 Mixed Integer Linear Programming

The lateral offset model makes it possible and fairly easy to realize centralized conflict resolution via the mixed integer linear programming.

Considering two aircraft streams as introduced previously, we assume that the number of aircraft is now finite (the two streams are truncated). The centralized optimization is that of minimizing the maximum lateral deviation experienced by any aircraft, subject to the constraint that all conflicts should be solved. Such an optimization problem may be easily written as a mixed integer programming problem, as follows. Referring to Fig. 5-1, aircraft A_i and A_j, assumed to travel at the same constant speed on orthogonal courses, will not be in conflict if and only if the protected circle A_i does not intersect the aisle projected by aircraft A_j. Let (x_i, y_i) and (x_j, y_j) be the coordinates of aircraft A_i and A_j and let d be the minimum allowable miss distance. A_i and A_j are not in conflict if and only if

$$
\begin{aligned}
x_i + y_i &\geq x_j + y_j + \sqrt{2}d \\
&\text{or} \\
x_i + y_i &\leq x_j + y_j - \sqrt{2}d.
\end{aligned}
\tag{5.1}
$$

These constraints are linear in the decision variables y_i and x_j, which are the lateral deviations for the eastbound and southbound aircraft, respectively. The centralized
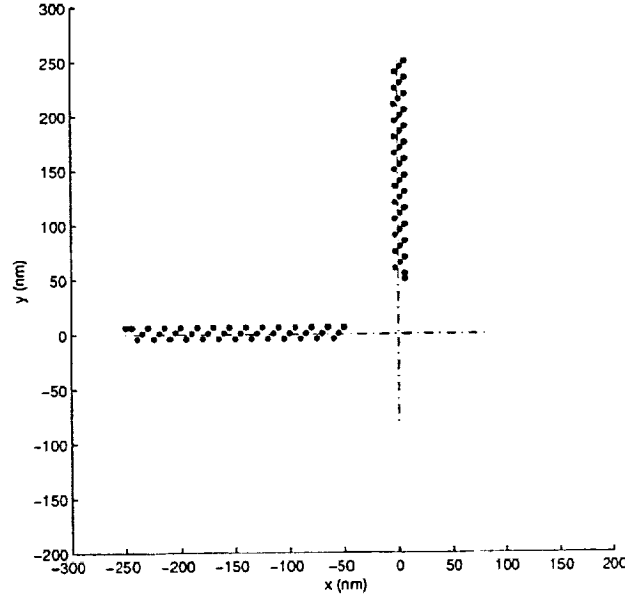
71

Figure 5-2: Conflict resolution for two streams of aircraft using the centralized algorithm under lateral offset model. The initial separation distance is 5 nm. The largest lateral displacement experienced by the aircraft is 6.1 nm.

conflict resolution problem may therefore be written as

$$\text{minimize} \quad \max\{\max_{A_i \text{ is eastbound}} |y_i|,$$
$$\max_{A_j \text{ is southbound}} |x_j|\} \tag{5.2}$$
$$\text{subject to} \quad (5.1).$$

This problem may be easily recast as a mixed-integer linear programming problem

$$\text{minimize} \quad \gamma$$
$$\text{subject to} \quad -\gamma \leq y_i \leq \gamma, \quad A_i \text{ is eastbound},$$
$$-\gamma \leq x_j \leq \gamma, \quad A_j \text{ is southbound}, \tag{5.3}$$
$$M t_{ij} + x_i + y_i \geq x_j + y_j + \sqrt{2}d,$$
$$M(t_{ij} - 1) + x_i + y_i \leq x_j + y_j - \sqrt{2}d,$$

where the continuous decision variables are y_i for the eastbound aircraft and x_j for the southbound aircraft, and t_{ij} are binary decision variables. x_i and y_j are fixed parameters, and M is a large constant. This problem may be solved efficiently using powerful linear programming optimization software such as CPLEX [7].

Fig. 5-2 shows the conflict resolution for the two streams of aircraft, with a total

72

of 82 aircraft. In this example, the initial separation distance between aircraft is $S = d = 5$ nm and the aircraft are initially configured as described in Fig. 3-6. Compared with Fig. 3-6, Fig. 5-2 reveals a slightly more compact conflict resolution structure: The largest lateral displacement experienced by the aircraft in Fig. 5-2 is 6.1 nm, which is slightly smaller than 7.1 nm, the largest displacement of aircraft in the decentralized test.

Similarly to problems involving two aircraft streams, it is possible to set up the centralized conflict resolution problem for three aircraft flows as a mixed integer linear programming problem. The same three aircraft flows as in Section 3.3 ($S = 5$ nm) have been truncated down to twenty aircraft per stream due to computational limitations.

Fig. 5-3 represents a snapshot of the aircraft flows after conflict resolution. The largest lateral displacement experienced by the aircraft is 23.1 nm, which is smaller than the maximum deviation experienced by the first 60 aircraft (20 in each stream) shown in Fig. 3-14, which is 60.7 nm. This indicates that for more than two intersecting aircraft flows, there may be considerable inefficiencies in aircraft conflict resolution amplitudes if they follow decentralized, strategies based on limited information.

5.1.2 Worst-case Performance Estimates for Centralized Resolution

In the previous subsection, we considered the centralized conflict resolution for lateral offset model. For general offset model allowing longitudinal displacement, we need to add a few more nonlinear and nonconvex constraints to problem (5.3):

$$(x_l - x_k)^2 + (y_l - y_k)^2 \geq d^2, \tag{5.4}$$

where aircraft with index l and k are in the same stream. Therefore, the centralized conflict resolution for offset model will in general need much more computation than the centralized resolution for lateral offset model. Besides getting exactly the optimal resolutions, we may predict the performance of centralized conflict resolution for offset
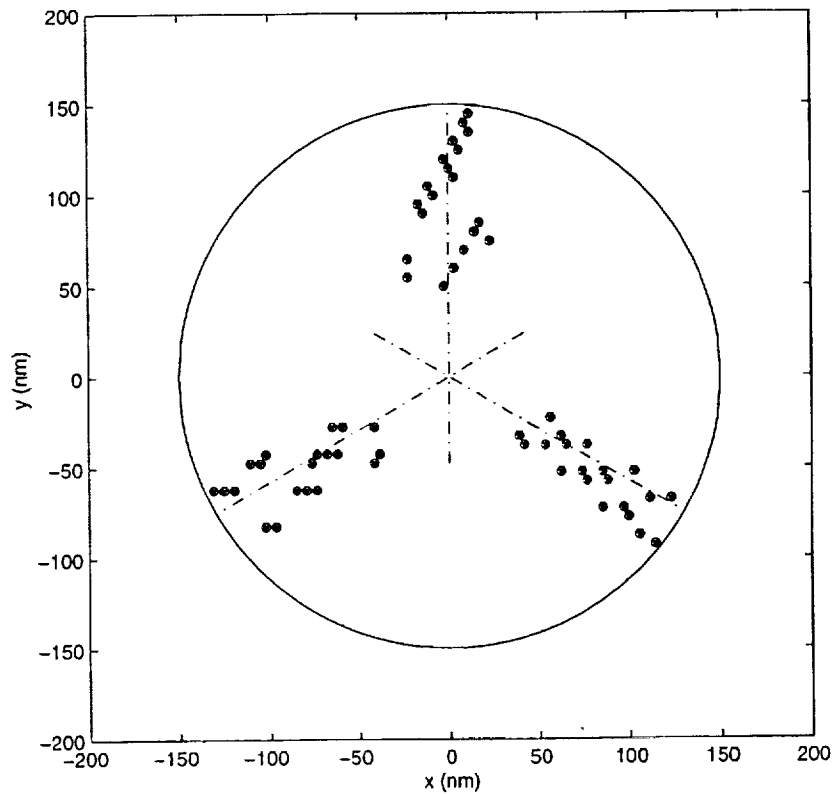
Figure 5-3: Conflict resolution for three streams of aircraft via the mixed integer linear programming under lateral offset model. The initial separation distance is 5 nm. The largest displacement experienced by the aircraft is 23.1 nm.
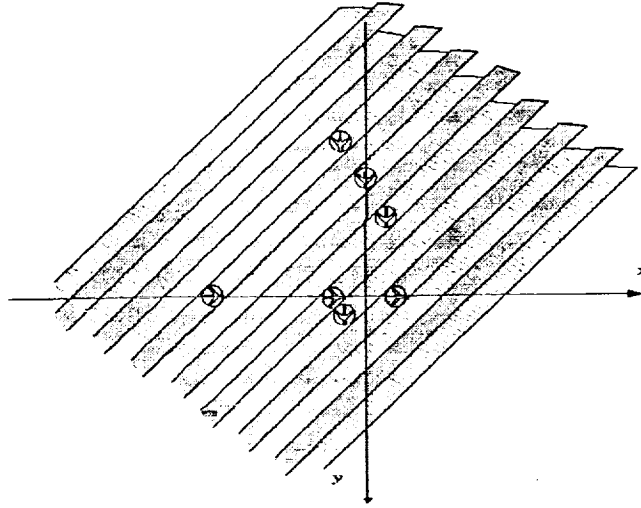
Figure 5-4: A way to partition airspace for two perpendicularly oriented aircraft streams.

model based on a study of conflict geometry of the aircraft flows.

Considering two intersecting aircraft streams, we know from the conflict geometry that the aisles of aircraft in both steams are parallel to each other. It is easy to see that the conflict resolution is equivalent to finding a partition of the airspace such that (1) the aisles of aircraft are distributed in a way where the aircraft from different streams will not overlap their aisles after resolution, and (2) the aircraft in the same stream with overlapped aisles should never overlap their protected circles. Since any feasible airspace partition described as above determines a solution to the centralized resolution problem, it determines an upper bound for the optimum value of the optimization problem for conflict resolution. In such sense, we may easily predict the performance of the centralized conflict resolution.

For example, Fig. 5-4 gives a way of partitioning airspace for two perpendicularly oriented aircraft streams. Considering the same conflict scenario of two aircraft flows as presented in Section 3.1, we can easily derive upper bounds for the largest lateral displacement of aircraft under the centralized conflict resolution, based on the partition in Fig. 5-4: For the lateral offset model, the bound is $\sqrt{2}d$; For the offset model allowing longitudinal displacement, the bound is $\sqrt{2}d/2$, only half the value of $\sqrt{2}d$ (note that $\sqrt{2}d$ is the largest lateral displacement we obtained in the decentralized resolution for the two aircraft flow problem in Section 4.1, Fig. 4-2). Obviously, this

partition will still apply when the aircraft streams have more density, *e.g.*, involving parallel aircraft.

The above idea of partitioning airspace can also be generalized to three aircraft streams. Note that in this case an aircraft projects two aisles, each of which is oriented along the relative velocity vector of this aircraft and the aircraft in one of the other two streams. As an example, Fig. 5-5 constructs a safe aisle distribution for three 120 deg oriented aircraft flows. The aisles in different streams have been identified with different darkness or patterns. From this construction, we see that the centralized conflict resolution strategies can always find an offset resolution with lateral position displacement no greater than $\frac{4\sqrt{3}d}{3} \approx 11.5$ nm (note that in the example of three aircraft flows under the decentralized resolution and offset model, as shown in Fig. 4-7, the largest lateral displacement of the 105 tested aircraft is 30.4 nm).
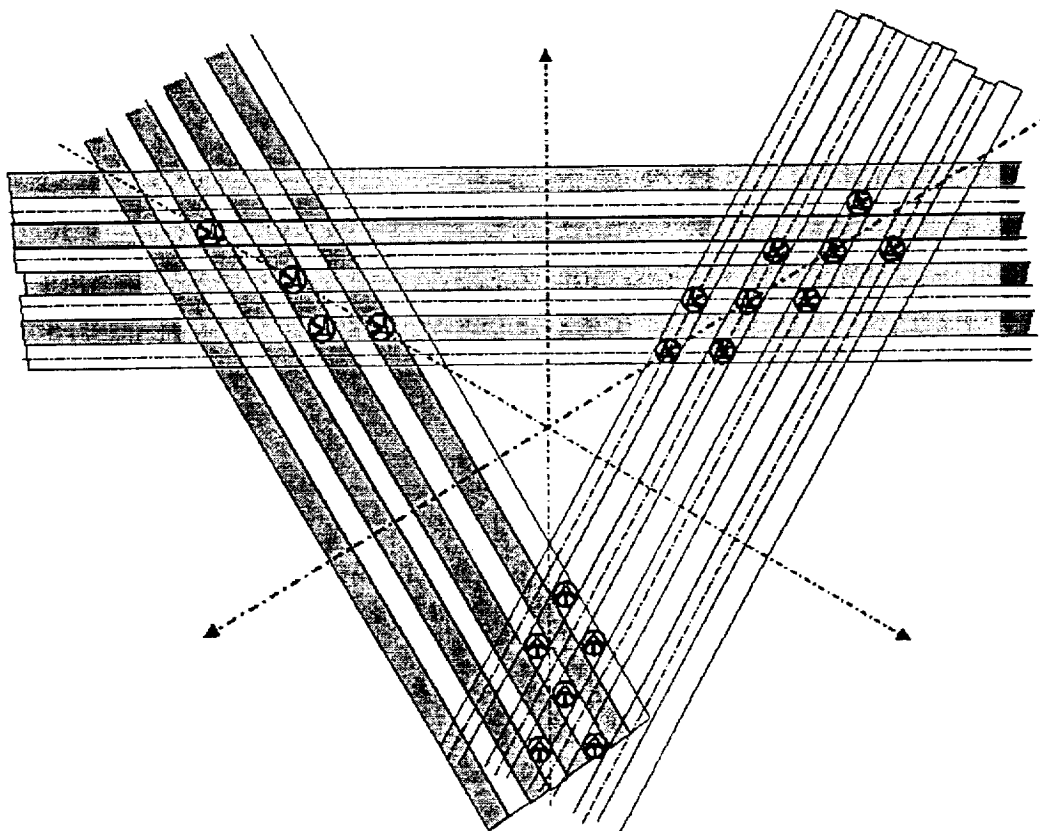
Figure 5-5: A way to partition airspace for three 120 deg oriented aircraft streams.

5.2 Centralized Resolution for Velocity Change Model

In our previous work [14], we have proposed an optimization algorithm for centralized resolution of conflicts involving multiple aircraft. The aircraft maneuver model is chosen to be the velocity change model, and the conflict resolution is based on semidefinite programming and random search. In this section, we use the mixed integer linear programming as the technique for centralized aircraft conflict resolution. This approach experimentally proves to run much faster than the one in [14].

5.2.1 Problem Formulation

Let n be the number of aircraft involved in one conflict and let each aircraft be identified by its index $i \in \{1, ..., n\}$. Denote the initial position of aircraft i by $\mathbf{p}_{i0}$ and its initial velocity by $\mathbf{v}_{i0}$. Denote its position at any time t by $\mathbf{p}_i(t)$ or the shorthand $\mathbf{p}_i$. Denote the commanded velocity changes by $\mathbf{u}_i$. We use a double-index notation for aircraft relative positions and velocities. Thus, the relative position $\mathbf{p}_{ij}$ is defined by $\mathbf{p}_{ij} = \mathbf{p}_i - \mathbf{p}_j$, and the relative velocity $\mathbf{v}_{ij}$ is defined by $\mathbf{v}_{ij} = \mathbf{v}_i - \mathbf{v}_j$. Further, $\mathbf{p}_{ij0} = \mathbf{p}_{i0} - \mathbf{p}_{j0}$ and $\mathbf{v}_{ij0} = \mathbf{v}_{i0} - \mathbf{v}_{j0}$. Denote d_{ij} as the miss distance between aircraft i and j.

There are three components in the optimization problem formulation for centralized conflict resolution: collision avoidance constraints, maneuvering constraints, and cost function.

Conflict resolution constraints can be expressed in many ways. In the present context, we express collision avoidance constraints in terms of a given *minimum miss distance*. Assume (i) a minimum safety distance d, (ii) no initial conflict between aircraft, and (iii) that aircraft follow straight trajectories at constant velocity. The conflict avoidance constraint is then shown graphically in Fig. 5-6 for a given aircraft pair (i, j) and can be written as $d_{ij} \geq d$, which is equivalent to

$$\mathbf{p}_{ij0}^T(\mathbf{v}_{ij0} + \mathbf{u}_{ij}) + ||\mathbf{v}_{ij0} + \mathbf{u}_{ij}||\sqrt{||\mathbf{p}_{ij0}||^2 - d^2} \geq 0, \qquad (5.5)$$
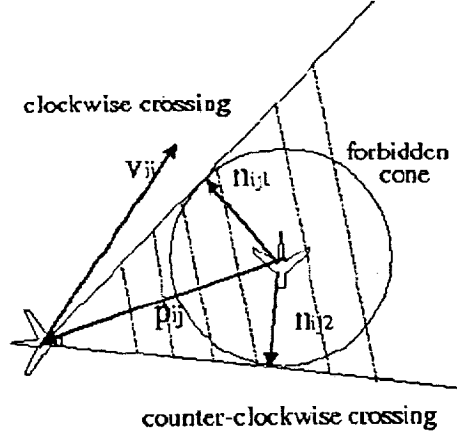
Figure 5-6: Conflict avoidance constraints for velocity change model.

where $\|x\|$ represents the Euclidean norm of vector x. As may be seen from Fig. 5-6, the conflict avoidance condition may be seen as the *union* of the half planes defined by the two linear constraints

$$(\mathbf{v}_{ij0} + \mathbf{u}_{ij})^T \mathbf{n}_{ij1} \geq 0 \qquad (5.6)$$

and

$$(\mathbf{v}_{ij0} + \mathbf{u}_{ij})^T \mathbf{n}_{ij2} \geq 0, \qquad (5.7)$$

where $\mathbf{n}_{ij1}$ and $\mathbf{n}_{ij2}$ are shown in Fig. 5-6.

The maneuvering constraints of an en route aircraft are significant. In particular at high altitude, the speed range of an aircraft is narrow. Usually, aircraft heading is not limited over the time scales under consideration. However, due to some specific flight conditions and consideration of passenger comfort as well as trajectory smoothness preference, we also need to put constraints on the heading changes sometimes. In the conflict resolution for the two aircraft flow problem, we restrict the velocity changes to stay within a given set around the current aircraft velocity: The set of possible changes is the convex set of possible velocity commands shown in Fig. 5-7. Denote $\mathbf{n}_{is}$ and $\mathbf{n}_{ih}$ as two unit vectors which are respectively parallel and perpendicular to the initial velocity vector of aircraft i. If the velocity deviation of an aircraft is small, then the velocity change along the direction of $\mathbf{n}_{ih}$ is for most part the result
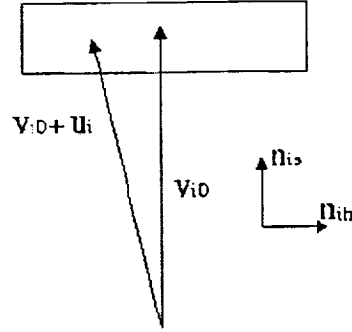
Figure 5-7: Maneuvering constraints for the two aircraft flow problem.

of the aircraft heading change, while the velocity change along the direction of $\mathbf{n}_{is}$ is mainly the consequence of the aircraft speed change. We write the resolution velocity command $\mathbf{u}_i$ as

$$\mathbf{u}_i = u_{is}\mathbf{n}_{is} + u_{ih}\mathbf{n}_{ih}. \tag{5.8}$$

It is easy to see that the constraint on $\mathbf{u}_i$ (shown in Fig. 5-7) is equivalent to the following constraints on u_{is} and u_{ih}:

$$|u_{is}| \leq u_{s,\max}, \quad |u_{ih}| \leq u_{h,\max}, \tag{5.9}$$

where the values of $u_{s,\max}$ and $u_{h,\max}$ are determined by the size of the "rectangle" in Fig. 5-7.

The cost function is chosen so as to minimize the velocity deviations from the original velocities or desired velocities. For the purpose of comparison with the decentralized resolution in Section 4.2, we use the following cost function for the aircraft flow problem:

$$J = \max_i \{t_i|u_{ih}|\}, \tag{5.10}$$

where t_i is the time to conflict for aircraft i. The above cost function is a measure of the maneuver corridor size of the aircraft flows.

5.2.2 Mixed Integer Linear Programming

Now we show that the optimization problem presented in the previous subsection can be formulated as a mixed integer linear programming problem:

- The constraint (5.5) (i.e., the union of the two linear constraints (5.6) and (5.7)) is equivalent to the following mixed-integer-linear constraints:

$$Mt_{ij} + (\mathbf{v}_{ij0} + \mathbf{u}_{ij})^T \mathbf{n}_{ij1} \geq 0,$$
$$M(1 - t_{ij}) + (\mathbf{v}_{ij0} + \mathbf{u}_{ij})^T \mathbf{n}_{ij1} \geq 0,$$
(5.11)

where t_{ij}'s are binary decision variables, and M is a sufficiently large constant.

- The cost function (5.10) is similar to the cost function of (5.2), and could be rewritten as

$$J = \gamma$$
(5.12)

together with a set of linear constraints

$$-\gamma \leq t_i u_{ih} \leq \gamma, \quad i = 1, ..., n.$$
(5.13)

Therefore, the optimization problem is to minimize the cost function (5.12) subject to constraints (5.13), (5.11) and (5.9). Obviously it is a mixed integer linear programming problem. As an example, we test the above formulation on a conflict resolution problem for two streams of aircraft, with a total of 18 aircraft. In this example, the initial separation distance between aircraft is 5 nm and the aircraft are initially configured as the example of Fig. 4-6 (right picture). Fig. 5-8 shows a snapshot of the centralized conflict resolution, which reveals a more compact conflict resolution structure than that of the first 18 aircraft shown in Fig. 4-6 (right picture). The largest heading deviation of aircraft is 1.62 deg in the example using centralized resolution, and is 3.78 deg in the example using decentralized resolution.
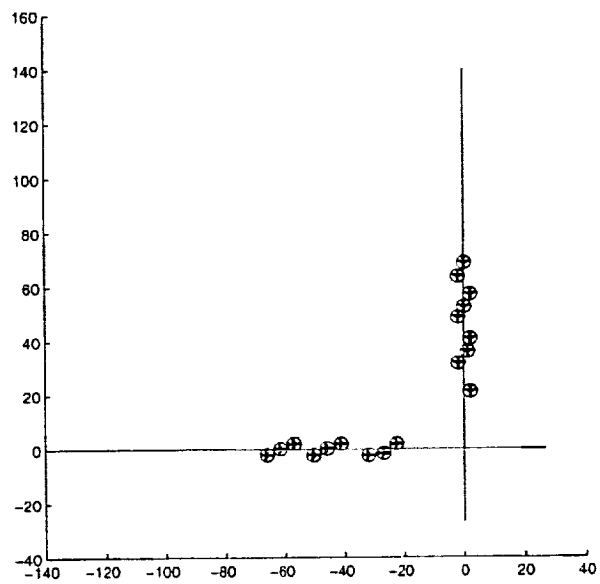
Figure 5-8: Conflict resolution for two streams of aircraft using the centralized algorithm under velocity change model. The initial separation distance is 5 nm.

Chapter 6

Conclusions

This thesis considers the problem of demonstrating stability of two interacting aircraft flows in a Free-Flight environment when these aircraft obey simple conflict resolution strategies. A new maneuver model with reduced complexity, the offset model, is proposed for analysis purposes, and has provided compact arguments establishing properties on the trajectories of aircraft after resolution. It is shown that this model is a very good approximation to the velocity change model, especially for small velocity deviations. Simulations are presented for both models to test the theoretical results as well as to generate some insight about the structure of the traffic flow after resolution.

It is shown for the lateral offset model (in Chapter 3) that the interacting aircraft flows remain stable under decentralized closed-loop conflict avoidance and derived a simple upper bound on the maximum deviation experienced by the aircraft. Numerical examples indicate the obtained bounds are consistent with the observed aircraft displacements. Then the arguments are extended (in Chapter 4) to general offset models with more control freedom for individual aircraft. Finally, a comparison is made (in Chapter 5) with centralized approaches to conflict resolution.

Further research effort will address the evolution of the interrelation between aircraft flow constraints and proposed centralized/decentralized conflict resolution systems.

Bibliography

[1] J.-M. Alliot, N. Durand, and G. Granger, "FACES: a free flight autonomous and coordinated embarked solver," FAA-Eurocontrol Air Traffic Management Seminar, Orlando, 1998.

[2] J. Andrews, "A relative motion analysis of horizontal avoidance," Technical Report, MIT, Lincoln Lab, 1978.

[3] D. Bertsimas and Y. Ye. Semidefinite relaxations, multivariate normal distributions, and order statistics, 1997.

[4] K. Bilimoria, H. Lee, Z. -H. Mao, and E. Feron, "Comparison of centralized and decentralized conflict resolution strategies for multiple aircraft problems," accepted, AIAA Guidance, Navigation and Control Conference, August 2000.

[5] J. Bobick, Improved Navigation by Combining VOR/DME Information with Air of Inertial Data, PhD Thesis, Stanford University, 1972.

[6] S. Boyd, L. El Ghaoui, E. Feron, and V. Balakrishnan. Linear Matrix Inequalities in System and Control Theory, vol. 15 of SIAM Studies in Applied Mathematics, SIAM, 1994.

[7] ILOG CPLEX user's guide, ILOG, 1999.

[8] S. Devasia and G. Meyer, "Automated conflict resolution procedures for air traffic management," Proc. 38th IEEE Conf. Decision and Control, Phoenix, Arizona, pp. 2456-2462, 1999.

[9] E. Dolginova and N. Lynch, "Safety verification for automated platoon maneuvers: a case study," International Workshop on Hybrid and Real-Time Systems (HART'97, Grenoble, France, March 26-28, 1997), vol. 1201, Lecture Notes in Computer Science, Springer-Verlag, pp. 154-170, 1997.

[10] J. Doyle, "Analysis of feedback systems with structured uncertainties," IEE Proc., vol. 129-D, no. 6, pp. 242-250, 1982.

[11] N. Durand, J.-M. Alliot, and O. Chansou, "An optimizing conflict solver for air traffic control," Air Traffic Control Quarterly, October 1995.

[12] M. S. Eby, "A self-organizational approach for resolving air traffic conflicts," The Lincoln Lab. Journal, vol. 7, no. 2, pp. 239-253, 1994.

[13] A. H. Epstein, "The inevitability of small" Aerospace America, no. 3, pp. 30-37, 2000.

[14] E. Frazzoli, Z. -H. Mao, J. -H. Oh, and E. Feron, "Resolution of conflicts involving many aircraft via semidefinite programming," to be published in Journal of Guidance, Control, and Dynamics.

[15] E. Gelenbe, Z. -H. Mao, and Y. -D. Li, "Function approximation with spiked random networks," IEEE Trans. Neural Networks, vol. 10, no. 1, pp. 3-9, 1999.

[16] E. Gelenbe, Z. -H. Mao, and Y. -D. Li, "Approximation by random networks with bounded number of layers," 1999 IEEE Workshop on Neural Networks for Signal Processing, Madison, USA, pp. 166-175, 1999.

[17] M. Goemans and D. Williamson, "Improved approximation algorithms for maximum cut and satisfiability problems using semidefinite programming," Journal of ACM, vol. 42, pp. 1115-1145, 1995.

[18] R. J. Hansman, "The national airspace system (NAS), how well do we know the plant?" SAE Control Systems Meeting, 1998.

[19] Honeywell, "Markets report," Technical Report NASA Contract NAS2-114279, Final Report for AATT Contract, 1996.

[20] S. Kahne and I. Frolow, "Air traffic management: evolution with technology", IEEE Control Systems Magazine, vol. 16, no. 4, pp. 12-21, 1996.

[21] J. Kosecka, C. Tomlin, G. Pappas, and S. Sastry, "Generation of conflict resolution maneuvers for air traffic management," IEEE Int. Conf. Intelligent Robots and Systems, Piscataway, NJ, vol. 3, pp. 1598-1603, 1997.

[22] J. Krozel, T. Mueller, and G. Hunter, "Free flight conflict detection and resolution analysis," AIAA Conf. Guidance, Navigation, and Control, San Diego, CA, 1996.

[23] J. Krozel and M. Peters, "Strategic conflict detection and resolution for free flight," Proc. 36th IEEE Conf. Decision and Control, San Diego, pp. 1822-1828, Dec. 1997.

[24] J. Krozel, M. Peters, and G. Hunter, "Conflict detection and resolution for future air transportation management," Technical Report, no. 97138-01, Seagull Technology, Inc., 1997.

[25] Z.-H. Mao, E. Feron, and K. Bilimoria, "Stability and performance of intersecting aircraft flows under decentralized conflict avoidance rules", accepted, 2000 AIAA Conf. Guidance, Navigation and Control, Aug. 2000.

[26] P. K. Menon, G. D. Sweriduk, and B. Sridhar, "Optimal strategies for free-flight air traffic conflict resolution," Journal of Guidance, Control, and Dynamics, vol. 22, no. 2, pp. 203-211, 1999.

[27] A. W. Merz, "Optimal aircraft collision avoidance," Joint Automatic Control Conf., Columbus, OH, pp. 449-454, 1973.

[28] Y. Nesterov and A. Nemirovsky. Interior-point Polynomial Methods in Convex Programming, vol. 13 of SIAM Studies in Applied Mathematics, SIAM, 1994.

[29] W. P. Niedringhaus, "Stream option manager: automated integration of aircraft separation, merging, stream management, and other air traffic control functions," IEEE Trans. Systems, Man, and Cybernetics, vol. 25, no. 9, pp. 1269-1280, 1995.

[30] J. -H. Oh and E. Feron, "Primal-dual quadratic programming approach to multiple conflict resolution," Proc. of American Control Conference, Philadelphia, pp. 2802-2806, 1998.

[31] R. A. Paielli and H. Erzberger, "Conflict probability estimation for free flight," Journal of Guidance, Control, and Dynamics, vol. 20, no. 3, pp. 588-596, 1997.

[32] M. Prandini, J. Lygeros, A. Nilim, and S. Sastry, "Randomized algorithms for probabilistic aircraft conflict detection," Proc. 38th IEEE Conf. Decision and Control, Phoenix, Arizona, pp. 2444-2449, 1999.

[33] N. Pujet and E. Feron, "Flight plan optimization in flexible air traffic environments," AIAA Conf. Guidance, Navigation, and Control, San Diego, CA, 1996.

[34] RTCA Task Force 3: Free Flight Implementation, Final Report, RTCA, 1995.

[35] R. W. Simpson, Course Notes for 16.72: Air Traffic Control, MIT, 1993.

[36] C. Tomlin, I. Mitchell, and R. Ghosh, "Safety verification of conflict resolution maneuvers," submitted to IEEE Trans. Intelligent Transportation systems.

[37] C. Tomlin, G. J. Pappas, and S. Sastry, "Conflict resolution for air traffic management: a study in multi-agent hybrid systems," Technical Report, University of California at Berkeley, 1996, also in IEEE Trans. Automatic Control, July 1998.

[38] C. Tomlin, G. J. Pappas, and S. Sastry, "Noncooperative conflict resolution," Proc. 36th IEEE Conf. Decision & Control, San Diego, CA, pp. 1816-1821, Dec. 1997.

[39] L. Vandenberghe and S. Boyd, "Semidefinite programming," SIAM Review, vol. 38, no. 1, pp. 49-95, 1996.

[40] P. Varaiya, "Smart cars on smart roads: problems of control," IEEE Trans. Automatic Control, vol. 38, no. 2, pp. 195-207, 1993.